Foreland basin magmatism in the Western Moroccan Meseta and geodynamic inferences

Martin Roddaz, Stéphane Brusset, Jean-Claude Soula, Didier Béziat, Mohamed Ben Abbou, Pierre Debat, Youssef Driouch, Frédéric Christophoul, Ahmed Ntarmouchant, Joachim Déramond

Foreland basin magmatism in the Western Moroccan Meseta and geodynamic inferences

Martin Roddaz,[1] Stéphane Brusset,[1] Jean-Claude Soula,[1] Didier Béziat,[1] Mohamed Ben Abbou,[2] Pierre Debat,[1] Youssef Driouch,[2] Frédéric Christophoul,[1] Ahmed Ntarmouchant,[2] and Joachim Déramond[1]

Received 20 July 2001; revised 21 February 2002; accepted 5 March 2002; published 9 October 2002.

[1] Basaltic magmatism occurs in the Hercynian foreland basin of the Western Moroccan Meseta as pillow lavas flows interbedded with ''flysch'' deposits and sills of dolerite and gabbro. A sedimentological and tectonic study shows that the deposition of the flysch, and thus the intrusion of the lava flows and sills, was controlled by the northwestward propagation of thrust-related folds in the wedge-top depozone of a syncontractional foreland basin system. The pillow lavas appear as either massive sheets of stacked lava flows or thin lava flows interlayered with the syntectonic turbiditic deposits. The sills are composed of several mafic units (up to six in the most evolved Marziqallal sill) cut through by granophyric veins, which can be interpreted as a result of in situ crystallization. The pillows lava basalts and the dolerites/gabbros are calc-alkaline and cogenetic. A discussion of the possible mechanisms of magma production in subduction related orogens leads us to conclude that this foreland basin magmatism was generated in a retrolithospheric setting. A comparison with the other Early Carboniferous volcanic and plutonic rocks of the Western and Eastern Mesetas shows that calc-alkaline foreland basin magmatism was widespread in the entire Mesetan domain and was probably a result of wet melting of the metasomatised mantle lithosphere of the overriding plate. Because the Moroccan Hercynides are likely to have been a result of continental subduction and the magmatism is observed at a distance of more than 500 km from the suture, it is suggested that the retroforeland basin magmatism was a result of either dehydration of a shallow dipping ($\sim$15°) foregoing oceanic slab, or underplating of the continental lithosphere ending with slab breakoff beneath the foreland basin. *INDEX TERMS:* 8102 Tectonophysics: Continental contractional orogenic belts; 8120 Tectonophysics: Dynamics of lithosphere and mantle—general; 8005 Structural Geology: Folds and folding; 3670 Mineralogy and Petrology: Minor and trace element composition; 9614 Information Related to Geologic Time: Paleozoic; *KEYWORDS:* retroforeland basin, pillow lava basalts, mafic sill, calc-alkaline, magmatism, continental subduction, Moroccan Meseta, Hercynian. **Citation:** Roddaz, M., S. Brusset, J.-C. Soula, D. Béziat, M. Ben Abbou, P. Debat, Y. Driouch, F. Christophoul, A. Ntarmouchant, and J. Déramond, Foreland basin magmatism in the Western Moroccan Meseta and geodynamic inferences, *Tectonics*, *21*(5), 1043, doi:10.1029/2001TC901029, 2002.

1. Introduction

[2] Foreland basins are a traditional field for studying the interplay, at different scales between tectonics and sedimentation during the construction of an orogen [*Ricci Lucchi*, 1986; *Catuneanu et al.*, 1997; *Miall*, 1997]. Although frequently related to extensional deformation till the years 85, foreland basins are now generally considered as syncontractional [e.g., *Allen et al.*, 1986; *Ricci Lucchi*, 1986; *DeCelles and Giles*, 1996]. Magmatism in syncontractional foreland basins is poorly documented. In the Veneto Region in front of the eastern Alpine foreland basin, *Milani et al.* [1999] have described basaltic magmatism including three magmatic series, tholeiitic, alkaline and transitional. Although its origin is still uncertain, this magmatism has been associated by these authors to a ''foreland reaction to the Alpine orogenic phase''. In the Volcanic Pyrite Belt (western Hercynian foreland basin, Iberia), *Mitjavila et al.* [1997] describe magmatic rocks ranging from tholeiitic basalts to calc-alkaline rhyolites interbedded with syncontractional sediments. The production of the basaltic magmas is ascribed to decompression melting of the asthenosphere resulting from local extension induced by syncontractional strike-slip shearing. In the Abor window (N. India), *Sengupta et al.* [1996] described syncontractional basaltic magmatism of Eocene age occurring in a shallow marine shelf environment in front of the Himalayan foreland basin. These basalts are chemically comparable to both Ocean Island Basalt (OIB) and Continental Flood Basalt (CFB), and their production is attributed to erosional decompression following lithospheric over-thickening [*Sengupta et al.*, 1996]. In the Ecuadorian Andes, *Barragan et al.* [1998] recognized calc-alkaline and shoshonitic magmatism in the active Sumaco volcano situated in the eastern Andean retroforeland foreland basin.

[1]Laboratoire de Mécanisme des Transferts en Géologie, UMR 5563, Université Paul Sabatier, Toulouse, France.
[2]Département de Géologie, Faculté des Sciences, Université Ben Abdallah, Fes, Morocco.

0278-7407/02/2001TC901029

This magmatism is interpreted as a result of dehydration of the subducting oceanic crust. In the western Alps, andesitic detritus of Eocene-Oligocene age are included in sandy turbidites, the Taveryannaz, Champsaur and Annot sandstones, issued from the orogen [*Sinclair*, 1997, 2000] and overlying the Globigerina Marls in the Swiss and French underfilled western proforeland basin [*Sinclair* 1997, 2000]. These detritus display calc-alkaline and shoshonitic trends [*Boyet et al.*, 2001] and have been interpreted as provening from volcanoes situated either in the proforeland basin (''autochthonous hypothesis'') [e.g., *Giraud and Didier*, 1981; *Boyet et al.*, 2001] or very close to and on both sides of the suture (''allochthonous hypothesis'') [e.g., *Von Blanckenburg and Davies*, 1995; *Sinclair*, 1997]. This magmatism has been ascribed either to partial melting of the upper plate metasomatized by subduction-induced dehydration of the downgoing plate and slab breakoff [*Von Blanckenburg and Davies*, 1995] or to slab breakoff causing partial melting of the subducting plate metasomatized during a previous orogenesis underneath the proforeland basin [*Boyet et al.*, 2001].

[3] The present paper deals with basaltic magmatism produced during the development of the Hercynian foreland basin of the Moroccan Meseta, which has been recently recognized as syncontractional [*Piqué et al.*, 1993; *Bouabdelli and Piqué*, 1996; *Ben Abbou et al.*, 2001]. The mafic rocks appear as pillow lava flows [*Kharbouch*, 1994] and widespread ''plutonic'' veins or sills (Ben Abbou, Roddaz, and N'Tarmouchant, unpublished data, 2000). The study presented herein is focused on the Fourhal area (northern Western Meseta) where the basaltic magmatism is best exposed and the relationship with the tectonic and depositional structures well apparent. These mafic rocks will be then compared with the other Visean magmatic rocks of the Moroccan Mesetas and the mechanism of emplacement, origin and geodynamic setting of this magmatism discussed on the basis of a comparison with the models of magma production in subduction-related orogens.

2. Geological Setting

[4] The Hercynian belt extends through various part of Morocco (Figure 1a). In southern Morocco, it comprises the mildly deformed Anti-Atlas belt, north of the West African craton; in north central Morocco, it is represented by the Western and Eastern Mesetas, several Paleozoic and Neoproterozoic inliers in the folded Mesozoic and Cenozoic cover of the Atlas and Rif domains [*Piqué and Michard*, 1989] and a rather large area ($\sim$150 $\times$ 150 km) of poorly deformed Visean sediments near Bechar on both sides of the Moroccan-Algerian frontier. The area more especially studied here is situated in the Moroccan Massif Central, which constitutes the north-central part of the Western Meseta (Figures 1a and 1b).

3. Structure and Sedimentation

[5] The Massif Central is usually described as a succession of large-scale synclines and anticlines (Figure 1b) originally defined by *Termier* [1936]. Recent structural studies [*Ben Abbou*, 2001; *Ben Abbou et al.*, 2001] have shown that the overall structure forms a north-west-vergent thrust wedge (Figure 2), the south-eastern termination of which is constituted by a duplex system developed between a basal décollement located in Middle Ordovician slates and an upper décollement constituted by the Silurian black shales (Figure 3). The upper part of this duplex constitutes the Azrou-Khenifra ridge as defined by *Termier* [1936]. At the wedge toe, the Visean paleofront situated in the northwestern flank of the Khouribga-Oulmes ridge, is constituted by a row of thrust-propagation anticlines, which controlled the deposition of the Late Visean marine sediments. These sediments, mainly thin turbidites and shales interdigited with large-volume and debris turbidity flow deposits were deposited as growth strata overlying terrains of Devonian to Early Visean age (Figure 3).

[6] In the central part of the wedge, thrusts and secondary backthrusts branching onto the upper décollement controlled the geometry of sub-basins filled with syntectonic deposits, the basal part of which was dated from fossil evidence of the Late Visean and Early Namurian (V3c, E1, E2)[*Ben Said et al.*, 1979, 1980]. The Addarouch, Abaqquar and Bou Idjaa (Ait Yazim) sub-basins in the Fourhal area have been more especially investigated (Figure 3). The Addarouch subbasin formed as a result of the overstep propagation of two branches of a NW-vergent thrust set. The Abaqquar sub-basin was controlled by a NW-vergent thrust-propagation fold associated with two SE-vergent passive backthrusts (passive roof duplex) [*Banks and Warburton*, 1986]. The Bou Idjaa sub-basin was controlled by a series of NW-vergent thrust-propagation folds. In these sub-basins, the control of deposition by propagating thrusts is shown by (1) the presence, at the base of the sub-basin-infilling sequences, of intra-formational unconformities geometrically linked to the structures induced by the propagation of the successive thrust faults and (2) a systematically retrograding catastrophic sedimentation issued from the forelimb of the folds abruptly interrupting the prograding normal sedimentation [*Ben Abbou et al.*, 2001].

[7] The mode of control of deposition by thrust-propagation folds is best illustrated by the example of the Addarouch sub-basin. The syntectonic deposits are there Late Visean- Early Namurian (Serpukhovian) in age. The catastrophic deposits (debris flows deposits, BT_2-T couplets of *Souquet et al.* [1987]) originated from reworking of the eastern limb as shown by the sedimentary structures and the nature of the included blocks. Toward the center of the sub-basin, these deposits are interdigited with the normal sedimentation represented by turbidite-like strata [*Walker and Plint*, 1992] probably affected by oscillatory currents [*Duke*, 1990]. To the northwest, the normal deposits are predominantly proximal storm-dominated deposits onlapping the backlimb of the Abaqquar anticline. In the Abaqquar and Bou Idjaa sub-basins, the normal sedimentation is similar but the catastrophic deposits become less coarse and more mature (Figure 4).

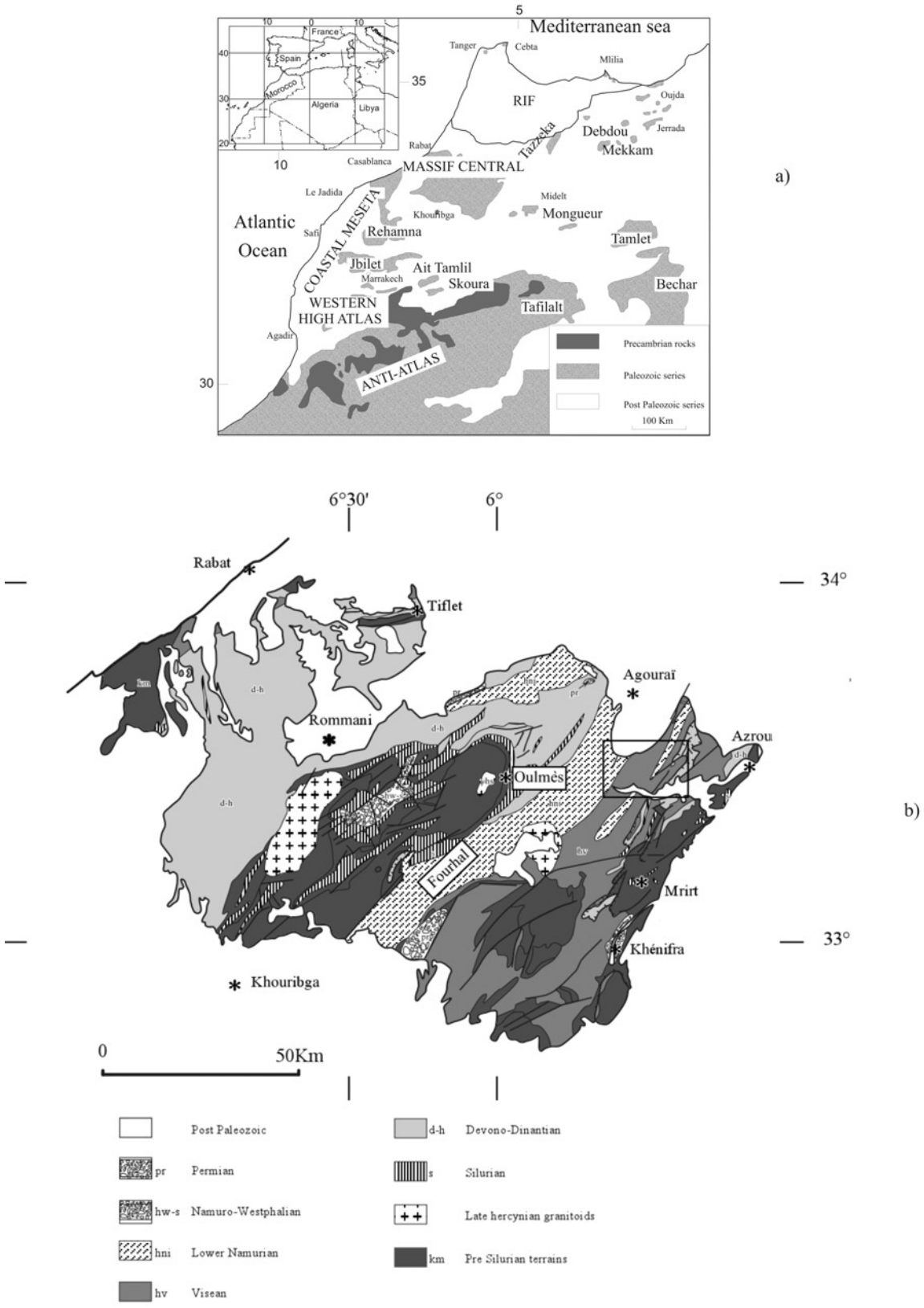

Figure 1. (a) Map of the Paleozoic outcrops in Morocco (modified from *Piqué and Michard* [1989]; reprinted by permission of American Journal of Science). (b) Geological map of the Moroccan Massif Central. The rectangle delineates the area shown in Figure 3.

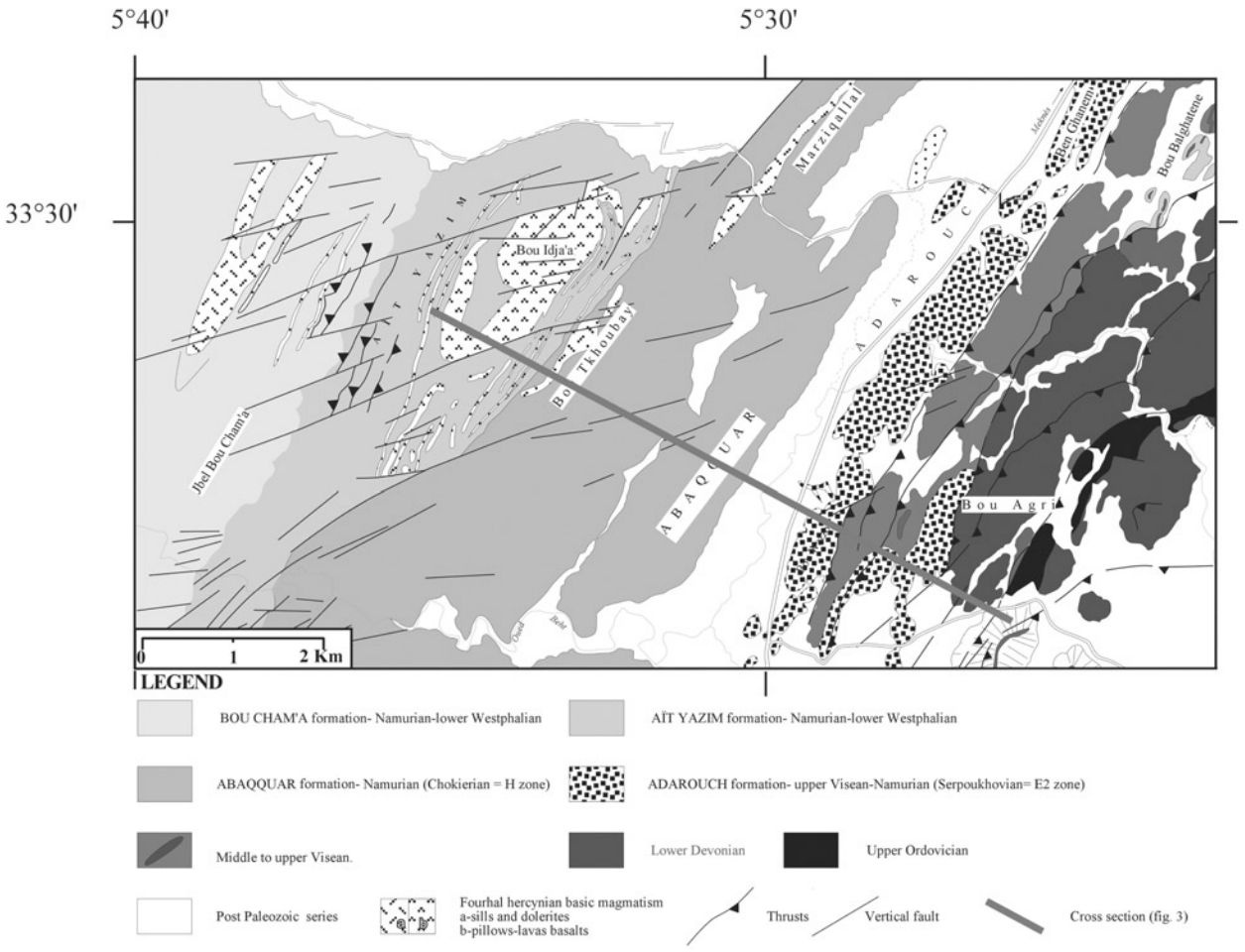

Figure 2. Geological map of Fourhal basin and location of the cross section of the Figure 3.

[8] Southwestward younging of syntectonic sedimentation and migration of the depocenters indicate a southwestward propagation of the thrust system. The Fourhal area can then be considered as a part of the wedge-top depozone of a foreland basin system [*DeCelles and Giles*, 1996], which extended at least over the present day Western and Eastern Mesetas [*Ben Abbou*, 2001; *Ben Abbou et al.*, 2001].

4. Basaltic Magmatism in the Fourhal Basin

[9] Basaltic magmatism is represented in the Fourhal area by pillow lava basalts [*Kharbouch*, 1994] and widespread gabbroic to granophyric sills or veins (M. Ben Abbou, M. Roddaz, and A. N'Tarmouchant, unpublished data, 2000). In the following, we will describe separately the volcanic sequence and the sills/veins. For each rock type, we will present successively (1) the mode of occurrence and the relationship with the depositional and tectonic structures, (2) the petrography and the mineralogy and (3) the chemical composition.

4.1. Analytical Techniques

[10] Fifty four thin sections have been examined under optical microscope and 36 modal analyses have been carried out. 135 electron-microprobe analyses were performed using a CAMEBAX SX 50 instrument at the Laboratoire de Minéralogie, Toulouse (beam current of 10 or 20 nA depending on the mineral's resistance to beam damage, 15 kV, with counting times of 10 s at peak positions and 5 s for backgrounds). The data were corrected using PAP (SX50) procedures (a list of the standard used is available from the authors upon request). Concentrations of major elements are accurate to 1 wt% of the element present, whereas concentrations of minor elements are less accurate, being reproducible to 0.1 wt. The modal and mineralogical data are available from the authors upon request. 23 rocks were analyzed by ICP-AES/MS for major elements and Nb, Rb, Y, Zr, Ba, Co, Cr, Ni and Sr at the CRPG, Nancy. The remaining elements were measured by ICP-MS at the Laboratoire de Géochimie of Toulouse. Three more analysis on Fourhal basalts have been performed at the CRPG of Nancy for trace and major

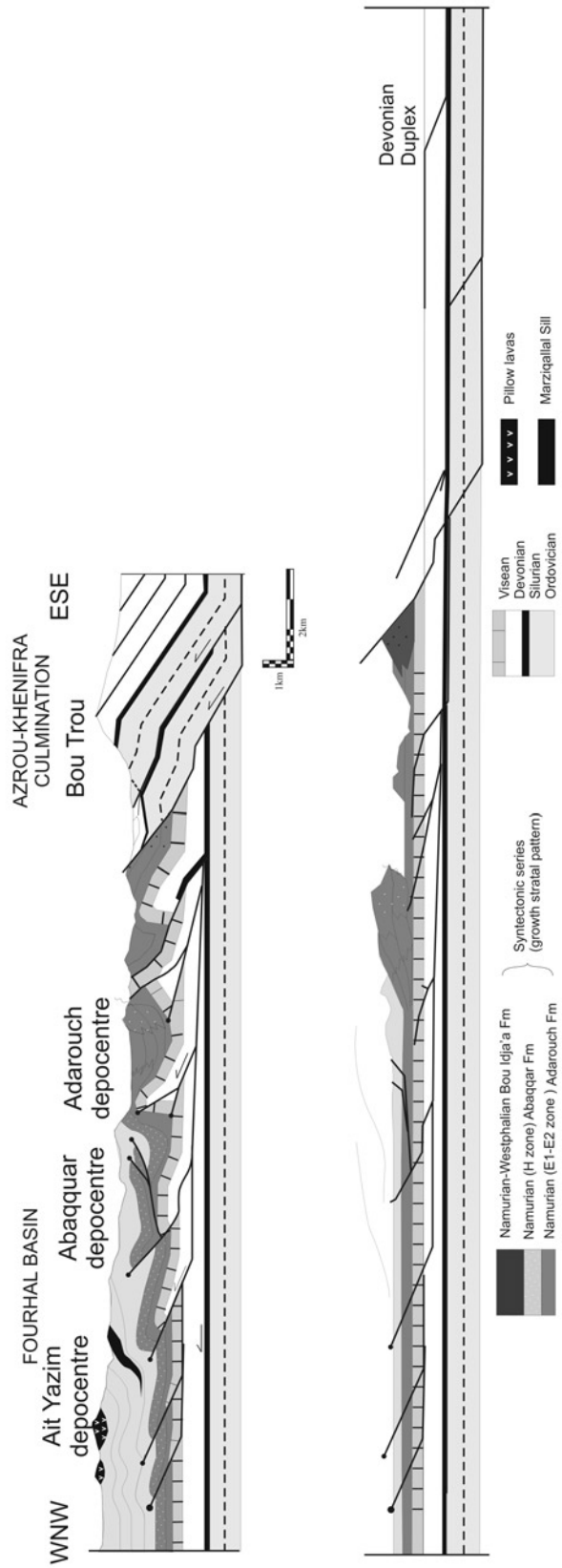

Figure 3. Balanced cross section of Fourhal basin structure.

Table 1. Representative Whole Rocks Analyses

	Unit 1, Gabbro				Unit 2, Olivine Gabbro		Unit 3, Gabbro					Unit 4, Gabbro	Unit 5, Ilmenite Gabbrodiorite			Unit 6, Amphibole Diorite	
	Mz1	Mz3	Maz1	Maz2	Mz5	Maz4	Mz8	Mz9	Maz5	Maz6	Maz7	Mz11	Mz13	Maz14	Maz15	Mz18	Maz16
Analysis	1	2	3	4	5	6	7	8	9	10	11	12	13	14	15	16	17
SiO_2	44.3	44.39	48.13	44.38	50.81	46.26	47.54	49	51.2	47.06	48.16	48.94	47.36	47.35	47.64	45.43	46.45
Al_2O_3	16.44	15.49	17.27	16.12	14.44	18.52	20.49	17.54	18.25	18.85	17.7	16.16	12.82	12.73	17.88	14.62	17.45
Fe_2O_3	10.03	9.68	8.24	8.91	11.28	8.12	8.43	8.85	6.69	8.05	8.49	8.19	15.14	16.29	9.17	10.3	10.15
MnO	0.16	0.14	0.13	0.13	0.19	0.11	0.11	0.14	0.09	0.12	0.13	0.13	0.25	0.23	0.14	0.14	0.15
MgO	8.21	11.6	8.1	8.94	8.47	8.44	5.54	6.32	5.27	8.09	7.37	7.31	3.78	4.3	6.35	12.04	8.24
CaO	10.9	9.33	10.48	10.64	10.33	9.3	8.52	11.3	7.14	10.34	11.35	12.52	7.74	8.84	10.68	9.43	9.02
Na_2O	2.25	2.12	2.94	1.81	1.87	2.41	3.43	2.96	4.69	2.38	2.51	2.68	3.77	3.24	2.82	2.57	2.9
K_2O	0.12	0.26	0.47	0.16	0.16	0.27	0.65	0.27	0.52	0.36	0.17	0.22	0.38	0.31	0.32	0.54	0.83
TiO_2	1.29	1.12	1.1	0.98	0.66	0.94	1.37	1.29	1.19	0.98	1.14	0.97	3.65	3.28	1.42	1.33	1.26
P_2O_5	0.24	0.2	0.21	0.17	0.15	0.19	0.19	0.23	0.3	0.17	0.2	0.16	0.4	0.31	0.24	0.2	0.2
LOI	5.92	5.57	2.86	7.65	2.05	5.31	3.62	1.98	4.53	3.46	2.66	2.57	4.61	3	3.21	3.3	3.25
Total	99.86	99.9	99.93	99.89	100.41	99.87	99.89	99.88	99.87	99.86	99.88	99.85	99.9	99.88	99.87	99.9	99.9
Mg≠	0.45	0.55	0.50	0.50	0.55	0.51	0.40	0.42	0.44	0.50	0.46	0.47	0.20	0.21	0.41	0.54	0.45
Sc	69	62	68	58	23	22	27	40	27	21	34	46	38	47	30	32	31
V	241	207	224	183	165	169	365	248	232	164	216	240	389	668	239	238	222
Cr	277	698	968	589	281	340	517	425	320	329	610	289	2	6	303	650	265
Co	46	59	38	57	69	43	27	33	21	40	37	34	36	47	35	56	45
Ni	151	373	141	289	336	181	69	56	50	225	95	59	7	11	93	343	147
Cu	214	163	148	118	209	256	149	285	131	156	198	225	355	458	402	147	393
Zn	150	79	60	76	118	255	83	97	53	64	68	63	150	140	76	101	88
Zr	95	74	88	68	53	58	91	68	126	63	76	57	197	166	76	71	69
Rb	2.69	7.92	17.95	5.22	6.93	11.12	27.51	6.05	19.71	13.15	4.06	6.37	11.10	9.81	10.19	14.00	25.13
Cs	1.48	1.35	6.89	1.51	4.04	2.44	2.70	0.83	3.00	1.66	1.12	2.16	3.17	2.81	1.69	1.19	1.92
Sr	283	302	383	261	174	309	320	226	332	322	205	210	227	207	223	186	267
Ba	52	100	130	71	55	135	209	80	199	143	63	58	122	175	107	98	287
Nb	1.21	0.37	0.60	0.07	2.14	2.04	2.73	2.88	4.83	2.33	2.54	2.00	8.94	6.55	3.61	3.14	2.24
Hf	1.98	1.29	1.73	1.24	1.37	1.35	2.25	1.79	3.05	1.47	1.83	1.45	4.66	4.16	1.86	2.00	1.70
Th	0.04	0.00	0.20	0.03	0.42	0.43	0.81	0.73	1.60	0.46	0.56	0.49	1.66	1.57	0.73	0.43	0.21
U	0.11	0.13	0.22	0.15	0.15	0.16	0.28	0.25	0.55	0.16	0.20	0.16	0.58	0.54	0.25	0.15	0.08
Y	25.32	20.24	24.31	18.73	16.26	16.79	22.74	25.04	43.39	16.85	21.06	20.34	53.04	47.78	26.08	26.58	22.66
La	4.11	3.89	5.07	3.58	3.41	3.86	5.51	5.49	11.45	4.05	4.55	3.77	12.62	10.93	5.87	4.72	3.44
Ce	11.77	10.54	13.41	9.81	9.16	10.26	14.82	14.73	30.51	10.62	12.21	10.33	33.74	29.16	15.81	13.41	10.06
Pr	1.88	1.63	2.06	1.51	1.38	1.51	2.13	2.21	4.37	1.54	1.80	1.58	4.91	4.29	2.33	2.06	1.59
Nd	9.90	8.44	10.45	7.80	6.87	7.50	10.36	10.92	21.11	7.69	9.19	8.13	24.52	21.28	11.61	10.50	8.52
Sm	3.10	2.64	3.12	2.44	2.07	2.23	3.02	3.31	6.13	2.22	2.73	2.55	7.09	6.35	3.46	3.31	2.71
Eu	1.20	0.98	1.10	0.90	0.84	0.90	1.26	1.25	1.50	0.95	1.04	1.00	2.37	2.05	1.24	1.12	1.07
Gd	3.90	3.13	3.79	2.89	2.62	2.77	3.67	4.08	7.21	2.77	3.42	3.21	8.66	7.84	4.32	4.12	3.56
Tb	0.69	0.54	0.66	0.50	0.44	0.46	0.62	0.70	1.21	0.46	0.59	0.56	1.46	1.33	0.73	0.71	0.61
Dy	4.51	3.59	4.37	3.36	2.92	3.06	4.19	4.68	7.91	3.05	3.85	3.73	9.72	8.93	4.76	4.80	4.08
Ho	0.95	0.73	0.93	0.71	0.62	0.63	0.87	0.97	1.62	0.63	0.79	0.77	2.02	1.84	0.98	1.02	0.86
Er	2.85	2.21	2.69	2.07	1.81	1.83	2.52	2.81	4.67	1.85	2.31	2.24	5.85	5.37	2.88	2.98	2.51
Tm	0.39	0.30	0.36	0.29	0.25	0.26	0.36	0.39	0.64	0.26	0.32	0.32	0.83	0.76	0.40	0.42	0.36
Yb	2.56	2.01	2.45	1.86	1.68	1.68	2.28	2.54	4.10	1.71	2.13	2.03	5.34	4.87	2.60	2.77	2.33
Lu	0.39	0.30	0.37	0.28	0.25	0.25	0.33	0.37	0.58	0.26	0.31	0.30	0.80	0.72	0.38	0.41	0.35
Ga	17.66	15.72	17.71	15.53	13.54	16.40	20.84	18.14	20.87	16.50	16.41	16.25	22.47	23.01	17.70	15.95	17.24
Ge	1.56	1.41	1.51	1.52	1.29	1.26	1.52	1.52	1.24	1.20	1.49	1.59	1.79	1.76	1.48	1.70	1.53

Table 1. (continued)

	Basalt					Granophyric Vein				Kharbouch's Basalt		
	Paz3	Paz1	Aiz1	Aiz7	Aiz9	Mz21	Mz4	Mz6	Maz9	1010	115	200
Analysis	18	19	20	21	22	23	24	25	26	27	28	29
SiO_2	48.31	54.22	46.3	53.23	50.89	62.82	58.04	72.57	53.48	51.06	50.06	50.8
Al_2O_3	17.13	17.17	17.07	16.36	17.79	14.84	15.69	13.45	15.5	14.84	16.82	14.55
Fe_2O_3	8.4	7.03	10.73	7.15	9.47	2.8	4.64	2.43	8.09	0.46	2.18	3.48
MnO	0.11	0.05	0.16	0.07	0.09	0.08	0.18	0.05	0.12	0.19	0.15	0.18
MgO	7.51	5.43	7.32	6.7	4.11	1.55	3.32	1.11	5.88	8.17	7.42	9.85
CaO	7.4	4.73	4.02	7.23	4.96	4.71	6.9	1.61	8.16	12.25	11.48	10.05
Na_2O	4.17	4.2	5.43	2.79	4.83	7.39	7.16	7.73	4.09	1.69	1.78	2.22
K_2O	0.74	1.9	0.13	0.61	1.24	0.06	0.15	0	0.26	0.49	1.09	0.4
TiO_2	1.55	1.35	1.9	1.55	1.38	0.68	2.64	0.35	1.09	1.06	1.07	1.03
P_2O_5	0.26	0.26	0.35	0.34	0.26	0.23	0.28	0.09	0.16	0.16	0.13	0.13
LOI	4.32	3.56	6.53	3.9	4.86	4.7	0.88	0.44	3.07	0.26	1.06	1.51
Total	99.9	99.9	99.94	99.93	99.88	99.86	99.88	99.83	99.9	99.5	99.92	100.66
Mg≠	0.47	0.44	0.41	0.48	0.30	0.36	0.42	0.31	0.42	0.47	0.46	0.50
Sc	33	24				52	57	42	57	37	30	38
V	263	211	282	262	271	78	414	6	207	274	231	262
Cr	204	45	246	209	7	37	29	4	384	243	165	206
Co	35	23	38	40	20	10	14	3	28	46	42	44
Ni	57	25	80	84	11	25	44	5	50	99	90	85
Cu	152	349	54	48	11	116	112	105	146	182	93	144
Zn	79	88	109	77	91	80	46	17	77	88	67	66
Zr	144	161	159	140	144	711	686	873	436	74	72	80
Rb	21.96	29.87	3.82	8.65	19.40	1.99	5.01	0.11	8.66	14.00	26.00	7.00
Cs	2.53	1.90	1.10	1.66	1.07	0.37	0.04	0.00	1.45	0.70	0.70	0.50
Sr	546	537	187	261	351	161	269	31	250	185	205	210
Ba	239	430	50	128	219	76	54	10	117	147	143	70
Nb	4.88	6.03	4.30	3.63	4.12	9.76	14.60	18.18	3.39	6.90	5.30	5.70
Hf	3.47	4.01	3.89	3.38	3.71	15.92	15.34	20.94	9.90	1.90	2.00	2.20
Th	1.87	5.84	1.93	1.93	4.87	3.38	5.40	8.57	3.13	1.20	1.50	1.30
U	0.62	2.71	0.63	0.60	1.42	1.38	1.97	2.91	1.23	0.40	0	0
Y	32.17	28.72	34.20	28.50	29.50	85.18	91.69	95.48	38.07	24.00	21.00	25.00
La	9.64	16.63	11.88	8.62	17.20	20.78	24.92	27.63	10.39	6.79	6.68	7.70
Ce	24.59	37.71	29.75	21.45	36.50	53.27	65.44	69.79	25.88	15.50	13.90	16.20
Pr	3.40	4.78	4.05	3.03	4.87	7.46	9.10	9.43	3.47	0	0	0
Nd	15.87	20.29	18.84	14.27	20.80	32.99	41.95	40.89	15.59	0	0	0
Sm	4.43	4.99	4.89	4.05	5.03	8.95	11.44	11.14	4.32	2.55	2.25	2.78
Eu	1.54	1.40	2.07	1.37	1.70	1.86	1.86	1.65	1.25	0.91	0.75	0.98
Gd	5.33	5.17	5.42	4.59	4.91	9.90	12.55	12.27	5.18	0.00	0.00	0.00
Tb	0.87	0.85	0.93	0.74	0.79	1.97	2.32	2.29	0.91	0.49	0.43	0.51
Dy	5.75	5.47	5.82	4.83	4.93	13.66	15.77	16.04	6.34	0	0	0
Ho	1.19	1.11	1.25	1.08	1.05	3.05	3.34	3.47	1.38	0	0	0
Er	3.45	3.25	3.39	2.83	2.99	10.11	10.26	11.12	4.25	0	0	0
Tm	0.48	0.47	0.54	0.43	0.40	1.55	1.48	1.71	0.66	0	0	0
Yb	3.21	3.13	3.68	3.23	2.95	10.74	9.74	11.66	4.39	1.70	1.51	1.85
Lu	0.47	0.47	0.53	0.46	0.42	1.66	1.41	1.76	0.67	0.31	0.26	0.32
Ga	19.29	19.55	20.50	17.70	24.00	32.33	20.38	24.01	16.75	16.50	16.41	16.25
Ge	1.35	0.98	1.93	1.28	1.12	1.34	1.59	1.60	1.52	1.20	1.49	1.59

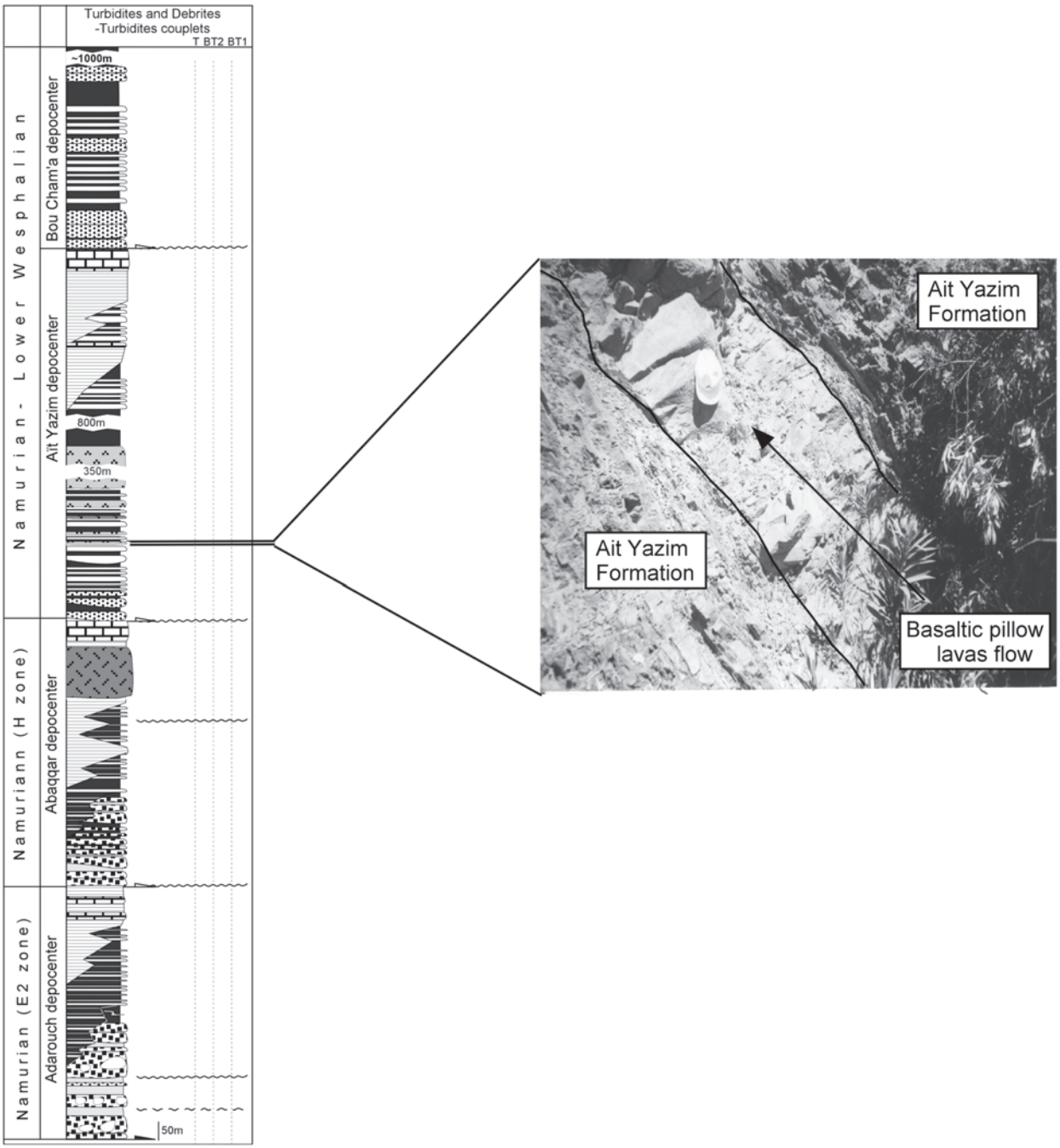

Figure 4. Simplified sedimentary column (modified from *Ben Abbou et al.* [2001]; reprinted with permission from Life Sciences).

elements. The compositions of these rocks are listed in Table 1.

4.2. Volcanic Sequence

4.2.1. Occurrence

[11] The volcanic sequence has been observed in the Ait Yazim Formation (Bou Idjaa syncline). It comprises a massive sheet of stacked pillow lavas (Figures 3 and 4) and several thin pillow lava flows interlayered with the syntectonic turbiditic deposits (Figure 3). These turbiditic deposits are here Early Namurian (Serpukhovian, E1-E2) in age [*Ben Said et al.*, 1979, 1980]. These rocks are all involved in the thrust-induced synsedimentary folds of the Bou Idjaa sub-basin which strike NE-SW, parallel to the

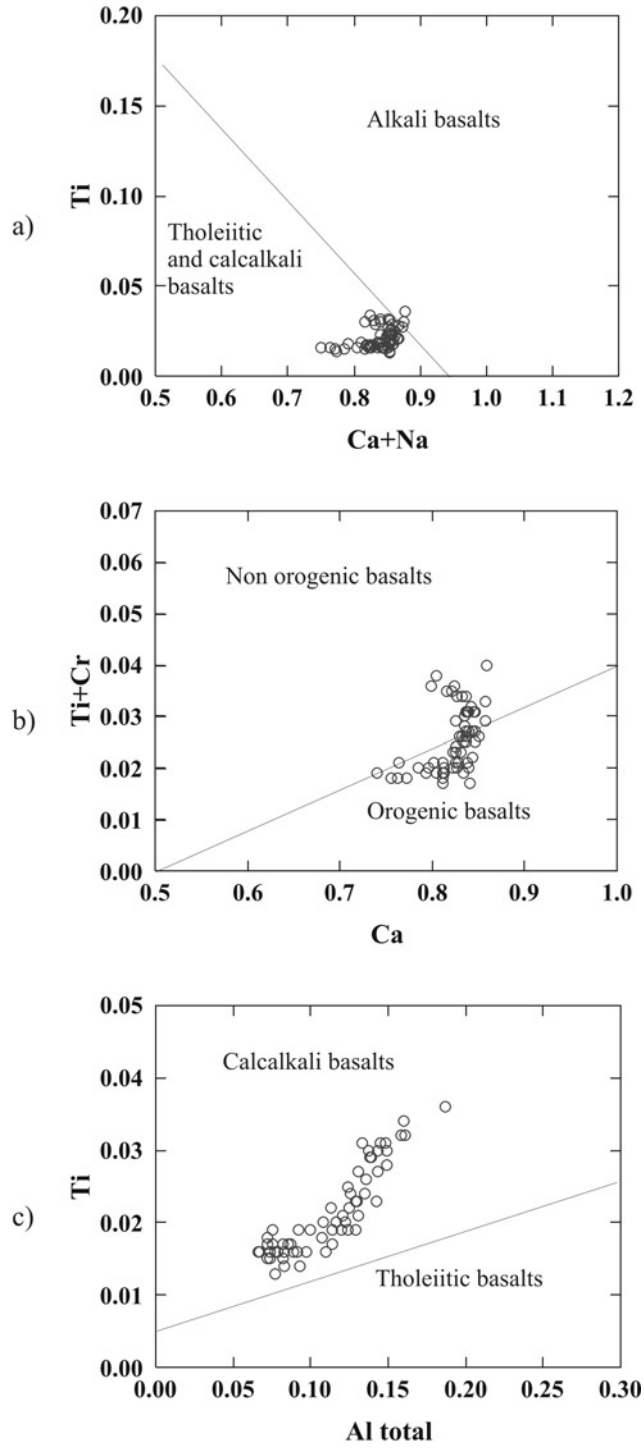

Figure 5. Discrimination diagrams of *Leterrier et al.* [1982] (reprinted with permission from Elsevier Science). (a) First discrimination diagram for clinopyroxene phenocrysts from alkali basalt and other basalts. (b) Second discrimination diagram for nonalkali basalts between nonorogenic tholeiites and orogenic basalts. (c) Third discrimination diagram for orogenic basalts between calc-alkali basalts and tholeiitic basalts.

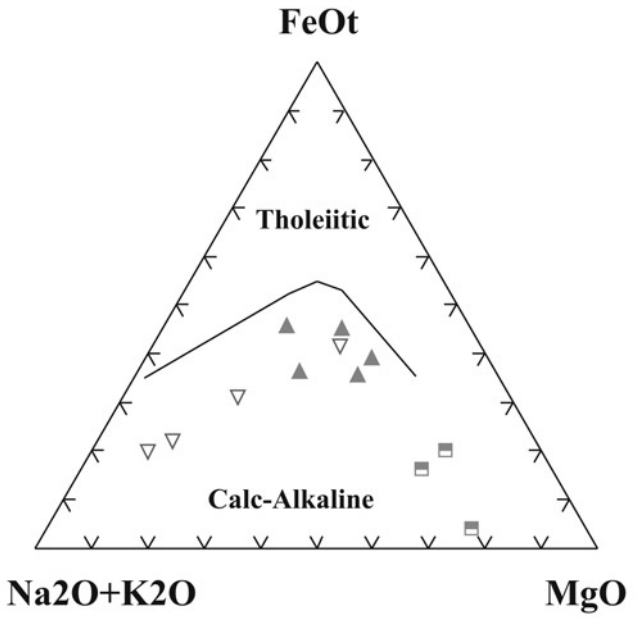

Figure 6. AFM diagram of *Irvine and Baragar* [1971]. Symbols are as follows: ▲ : basalts; ▽ : granophyric vein; ▬ : basalts analyzed by *Kharbouch* [1994].

trend of the range. The relationship between these deposits and the tectonic structures described above demonstrates that the pillow lava basalts erupted in front of propagating thrust-related folds and are therefore contemporaneous with the formation of the syncontractional foreland basin.

4.2.2. Petrography and Mineralogy

[12] The thick pillow lava sheet situated at the central part of the flow (Paz1) is seriate-textured with phenocrysts of plagioclase and clinopyroxene (up to 1 cm across) whereas basalts from the lower or upper part of the flow (Paz3) are porphyritic with plagioclase and clinopyroxene phenocrysts set in a fine grained intergranular groundmass of acicular plagioclase. The thin pillow lava sheet (AIZ1, AIZ7, AIZ9) interbedded with Ait Yazim sediments display the same porphyritic texture as the massive bed. All these basalts exhibit interstitial ilmenite.

[13] Clinopyroxene occurs in both types of basalts. Its composition varies from Mg-Augite to Fe-Diopside. Plots of 68 Clinopyroxene analyses in *Leterrier et al.*'s [1982] diagrams show unambiguous affinities with clinopyroxenes from calc-alkali basalts and orogenic basalts (Figure 5).

[14] Plagioclase is always pseudomorphosed into albite, white micas or epidote.

[15] Ilmenite occurs in a small quantity. Its composition is the same in both types of basalts.

4.2.3. Geochemistry

[16] Because low-grade alteration assemblages are observed in all the basalts, our study was focused on those elements which are generally considered as immobile during secondary processes (elements of intermediate ionic potential in their common oxidation states, i.e., Ti, Zr, Hf, Nb, P, Th, Y and REE).

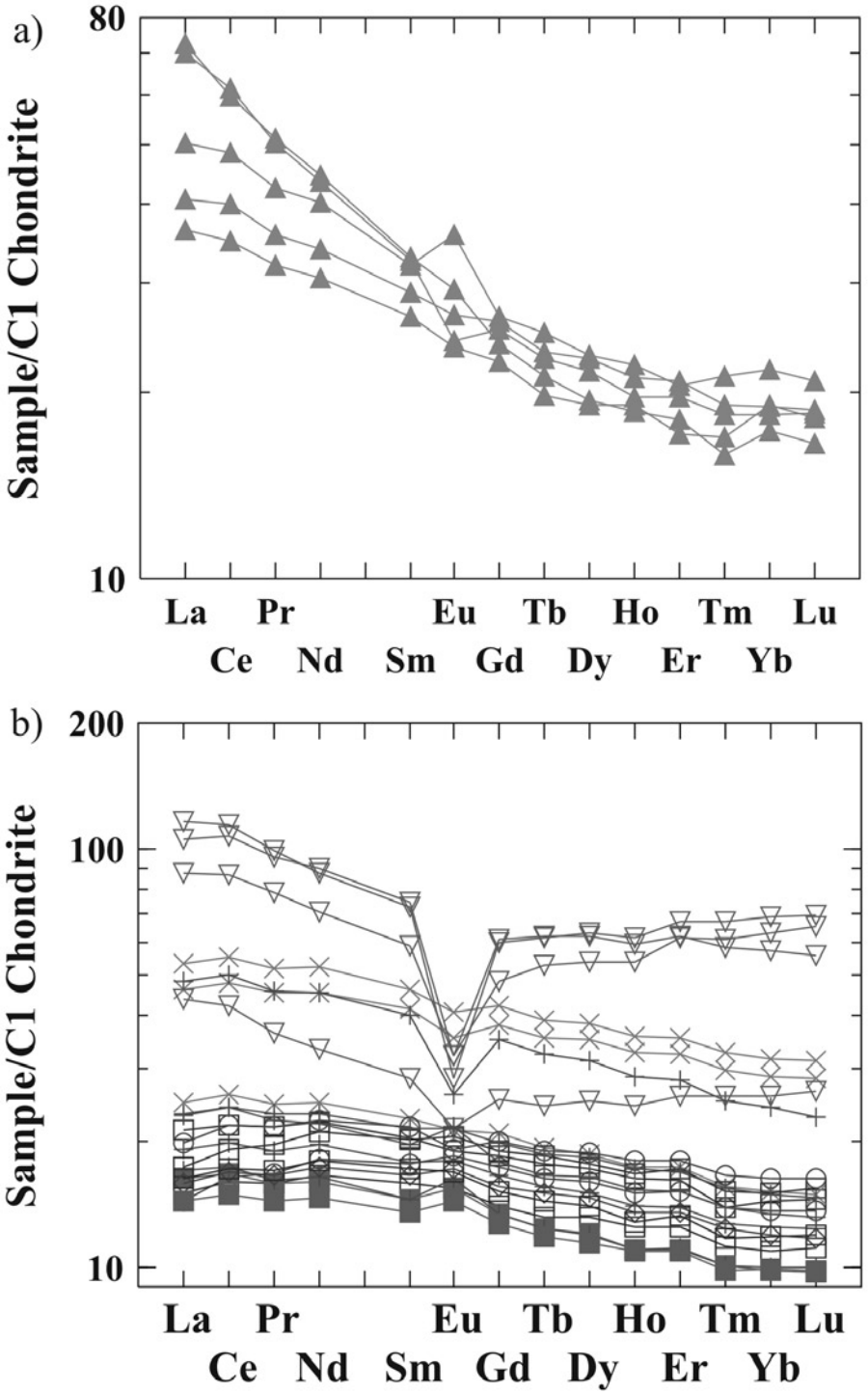

Figure 7. Concentrations of the rare earth elements (REE) for the Fourhal volcanic sequence (a) and the Marziqallal rocks (b). C1 chondrite values of *Sun and Mc Donough* [1989]. Symbols are as follows: □ : Unit 1 (Marziqallal sill); ■ : Unit 2; + : Unit 3; ◇ : Unit 4; × : Unit 5; ○ Unit 6; See Figure 6 for other symbols.

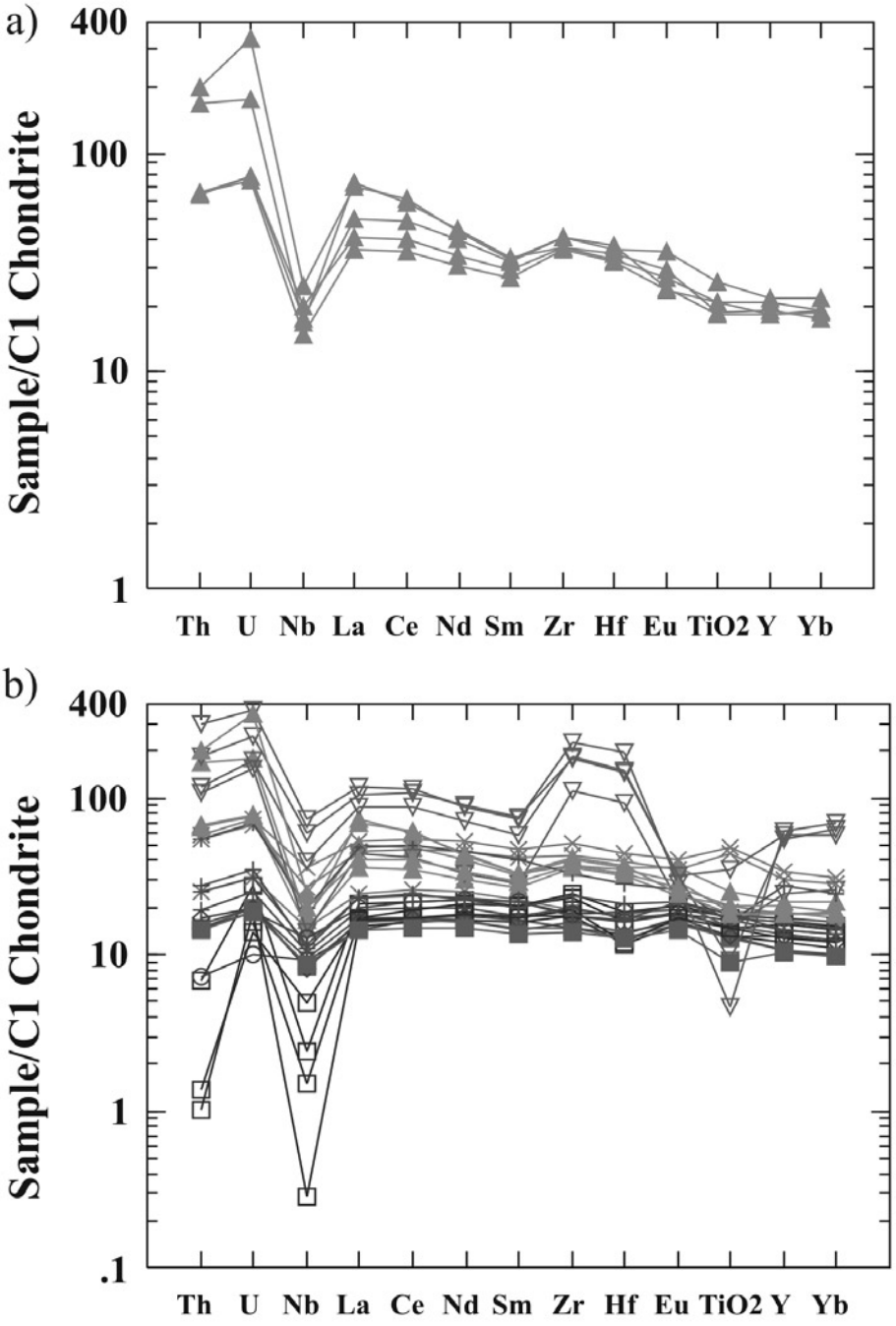

Figure 8. C1 chondrite-normalized multi-element diagram for the Fourhal volcanic sequence (a) and the Marziqallal rocks (b). Normalization values of *Sun and McDonough* [1989]. See Figures 6 and 7 for symbols.

[17] The rock sequence of the Fourhal area consists of a calc-alkaline suite in terms of *Irvine and Baragar*'s [1971] criterion of total alkali-total Fe (expressed as FeO*)-MgO (AFM diagram) (Figure 6). Most of these basalts are significantly fractionated, with low MgO (<7.5%), Mg-number <50, and low Ni (<60 ppm). Chondrite-normalized abundances of the REE (Figure 7a) in the Fourhal basalts are (20–70) X chondrite and are light-REE-enriched with $(La/Yb)_N = 2–4$, similar to those reported in many calc-alkaline basalts, e.g., Ruapehu and Egmont lavas in northern New Zealand [*Smith et al.*, 1997]. Two samples are still more enriched in LREE. On a chondrite normalized multi-element plot (Figure 8a), the basalts exhibit patterns typical of many subduction zone magmas, with Th, U enrichments

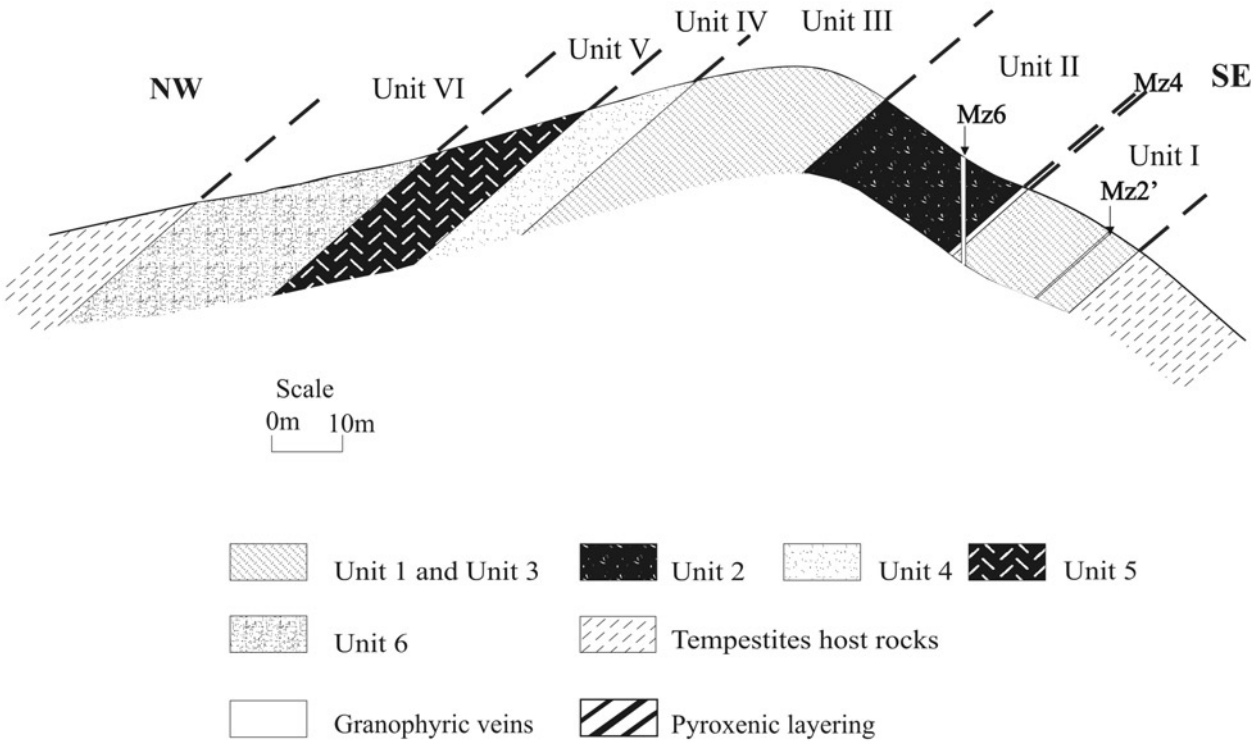

Figure 9. Simplified cross section of Marziqallal sill.

and Nb, Ti depletions, e.g., Okmok lavas, central Aleutians [*Nye and Reid*, 1986].

4.3. Sills and Veins

4.3.1. Occurrence

[18] Numerous dolerite veins, several meters thick and several hundred meters long, occur in Ait Yazim and Bou Chama'a formations. Two gabbro sills (Marziqallal and Bou Thoukbay) with similar dimensions (approximately 3 km long and 150 to 200 m thick), crop out in the Abaqqur formation. These sills and veins in general intruded parallel to bedding, and less frequently along thrust-related faults, and are folded by younger thrust-related folds formed as a result of the propagation of the thrust wedge. These sills and veins are also frequently necked and the spacing of the necks varies from less than 1 m to 10 m or more as a function of the thickness. At outcrop scale, the boundaries with the host rocks are planar [*Irvine*, 1982] with no contact metamorphism or deformation, which strongly suggests a rapid intrusion at high temperature and low crystal content. These observations bear evidence that the mafic sills and veins emplaced during the development of the Fourhal sub-basin and are thus Late Visean to Early Namurian in age.

4.3.2. Petrography

[19] The dolerite veins display a typical doleritic texture with plagioclase and clinopyroxene phenocrysts and no significant changes can be observed from one vein to another.

[20] The Marziqallal sill (150 m thick) is composed of six different mafic units and various granophyric veins (Figures 9 and 10). All units are made of basic cumulate and exhibit thin uniform layers (0–5 cm thick). The crystallization sequence inferred from cumulates is: plagioclase ± spinel + olivine + clinopyroxene + ilmenite + amphibole + biotite + quartz. Unit 1 is 20 meters thick. It is composed of gabbros (samples Mz3, Maz2 and Maz1) with an apparently chilled margin (Mz1) at the bottom of the sill (1 m). These gabbros contain abundant euhedral plagioclase (up to 2 cm across) as cumulus mineral (up to 67 vol%). The post-cumulus minerals are predominantly clinopyroxene (about 33 vol%) with xenomorphic poikilitic habitus (up to several centimeters) and ilmenite (about 1 vol%). This unit can be thus interpreted as orthocumulate gabbros [*Irvine*, 1982]. Unit 2 (samples Maz4 and Mz5) is 20 meters thick. The cumulus minerals are plagioclase (45 to 65 vol%) and sub-rounded olivine (5 to 28 vol%). Plagioclase crystallized prior to olivine. The post cumulus minerals are essentially poikilitic clinopyroxenes (about 20 vol%), ilmenite (about 3 vol%) and biotite (1 vol%). Olivine is concentrated in a ~50 cm thick horizon. Unit 2 also presents thin layers of clinopyroxene and plagioclase is concentrated near the base. This unit is therefore made up of orthocumulate olivine gabbros. Unit 3 (samples Mz8, Mz9, Maz5, Maz6 and Maz7) is 40 meters thick. The cumulus mineral is euhedral plagioclase (60 to 80 vol%). The post cumulus minerals are clinopyroxene (17 to 35 vol%) and ilmenite (3 to 5 vol%). It must be noticed that inter-cumulus volume increases topward. Unit

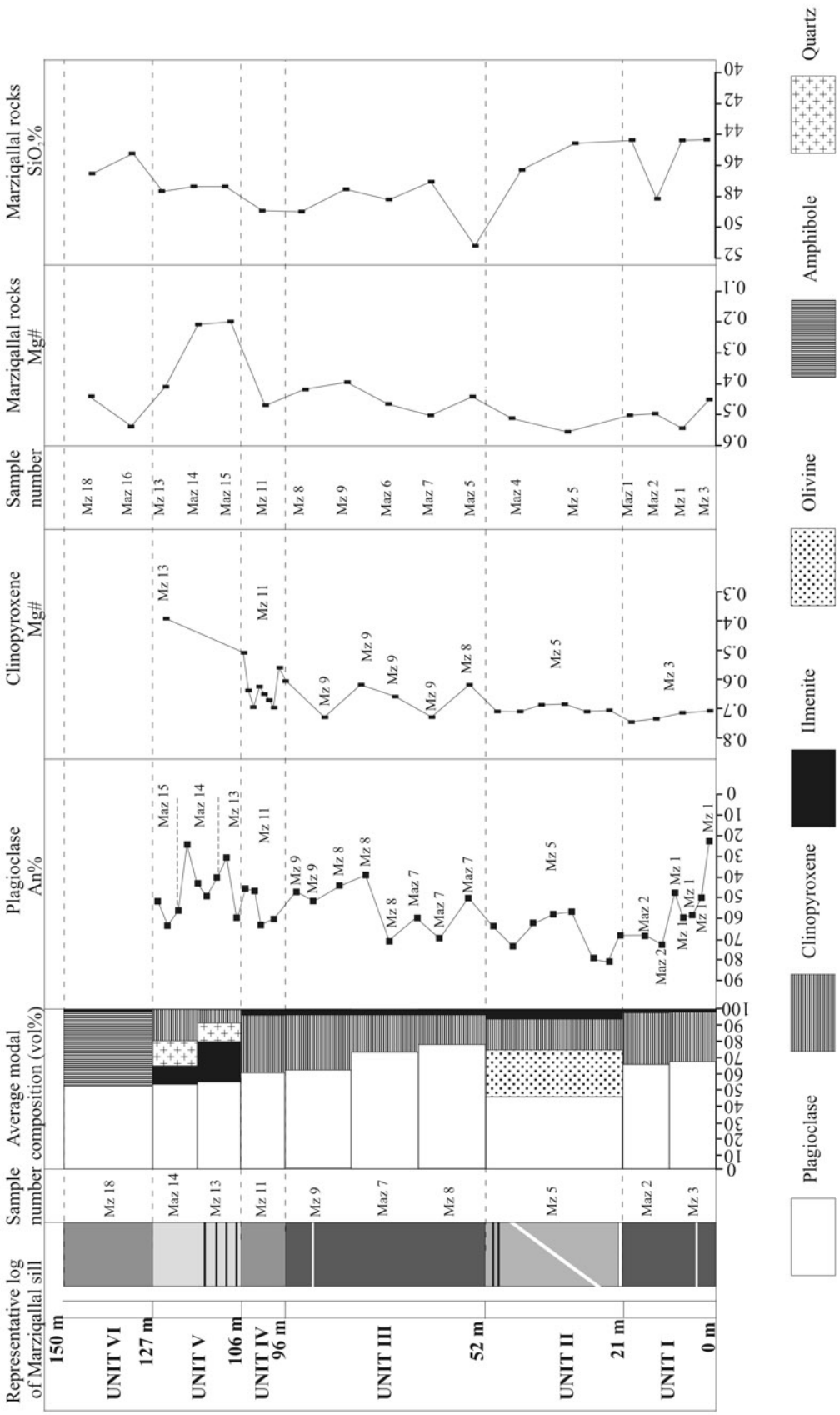

Figure 10. Lithology, modal composition, variations of mineralogical composition, and variations in chemical compositions in oxides of the six units of Marziqallal sill (clinopyroxene $Mg\# = Mg^{2+}/(Mg^{2+} + Fe^{2+})$.

3 is therefore composed of orthocumulate to mesocumulate gabbros. Unit 4 (sample Mz11) is 10 meters thick. It has the same characteristics as unit 3 except that a small amount of quartz (0.5 vol%) occurs in a post-cumulus position. Thus, unit 4 is composed of orthocumulate gabbros (±quartz). Unit 5 (samples Mz13, Maz14 and Maz15) is 15 meters thick. The cumulus minerals are plagioclase (∼55 vol%), and ilmenite (up to 25 vol%) forming 2 cm wide patches that display intergrowth features with plagioclases. Clinopyroxene (10 to 30 vol%) and quartz (7 vol%) constitute the post cumulus minerals. Magmatic reactions between quartz and plagioclase are attested by the presence of myrmekites (2 to 8 vol%). Unit 5 is therefore made of orthocumulate ilmenite gabbrodiorite. Unit 6 (sample Maz16) is ∼10 meters thick, and shows an apparently chilled top-margin (sample Mz18). It is characterized by the appearance of subeuhedral amphibole as a post cumulus mineral (up to 45 vol%). Plagioclase is always the cumulus mineral. It appears in laths, often sericitized. Unit 6 is therefore composed of orthocumulate amphibole diorite. Four granophyric veins (samples Mz21, Mz4, Mz6 and Maz9) 2 cm to 1 m thick, cut through the sill (Figures 6 and 7). The contacts with the host rock are planar. These veins usually show pegmatitic texture with plagioclase megacrysts (1–2 cm), euhedral clinopyroxene, ilmenite and occasionally quartz and myrmekites.

[21] The Bou Thoukbay sill is composed of equivalents of the Marziqallal Units 1 and 3 and displays the same characteristics as these units.

4.3.3. Mineralogy

[22] Clinopyroxene occurs in all the Marziqallal units except Unit 6. The composition varies from Fe-Augite ($Wo_{47}En_{48}Fs_{53}$) to Mg-Diopside ($Wo_{50}En_{86}Fs_{14}$). In order to evaluate the differentiation in the sill, the Magnesium number Mg# = 100 [$Mg^{2+}/(Mg^{2+} + Fe^{2+})$] of clinopyroxene has been plotted as a function of the distance to the base of the sill (Figure 10). The diagram shows that the differentiation increases in Unit 5 where Cpx Mg# varies from 0.95 to 0.8, which is correlated with the observed mineralogical evolution and the unusual abundance of quartz.

[23] Plagioclase presents a normal zonation except in the diorite of Unit 6 where it is always pseudomorphed into albite, white micas, epidote or calcite. When plotting the percentage of anorthite in the different petrographic units (Figure 10), we note a decrease in An_{max} concomitant with the decrease in Cpx Mg#.

[24] Olivine is one of the cumulus minerals of Unit 2. It is well preserved and forms subrounded crystals, which are unzoned and show a limited compositional variation (Fo76–Fo75).

[25] Ilmenite occurs in all the units of the Marziqallal sill, and only small variations in composition are observed.

[26] Brown amphibole occurs in Unit 6 as a magmatic post-cumulus mineral. Using IMA nomenclature (1997), it ranges in composition from Magnesio-Hastingsite to Edenite-Hornblende. Secondary amphibole developed mostly from clinopyroxene and its composition varies from tremolite to actinote.

[27] Biotite is rare and is always found in a post cumulus position. It is rich in magnesium (up to 80% phlogopite).

[28] Spinel occurs as rectangular crystals in olivine from Unit 2 of the Marziqallal sill and has a composition of chromite.

4.3.4. Chemical Composition of Whole Rock Units and Veins

[29] The variations in SiO_2 content are small in the mafic rocks of the Marziqallal sill (Figure 11). Unit 3 has the highest SiO_2 content (49 wt.%) whereas unit 1 and unit 2 have the lowest one (44 to 45%). In the granophyric veins, the values in SiO_2 content are markedly higher and range from 55 to 75 wt%. A correlation is also observed between the variation of the Mg number in clinopyroxene and in the whole rocks with a minimum corresponding to Unit 5 (Figure 10). In the chondrite-normalized rare earth element (REE) patterns (Figure 7b), the cumulates show flat parallel patterns except Unit 5, which is REE enriched and, like granophyric veins, show a Eu negative anomaly. On a chondrite-normalized multi-element plot, both cumulate and granophyric veins display similar negative Nb anomalies, negative to positive anomalies in Th and Eu. The granophyric veins show positive anomalies in Zr and Hf (Figure 8b)

[30] Although all the rock units found in the Marziqallal sill are not present, the Bou Thoukbay sill displays the same chemical characteristics (Y. Driouch et al., manuscript in preparation, 2002).

4.3.5. Origin of the Sills

[31] The characteristics of the Marziqallal sill could be explained either by multiple injection or in situ crystallization. Multiple injections might explain the mineralogical diversity but is precluded by the cumulus framework of the rocks and the small variations in chemical composition of rocks and minerals. In situ crystallization is supported by the unchanged composition of plagioclase, ilmenite, clinopyroxene and amphibole, the small variation in SiO_2 (Figure 11) content and the parallelism of the REE (Figure 7b) patterns. All the chemical variations are mostly controlled by the mineralogy. The TiO_2 and FeO^t contents are higher in unit 5 (Figure 10), which is consistent with the fact that ilmenite is there a cumulus phase. This may explain why this unit has the lowest MgO content and Mg number. Unit 2 has the highest MgO content because of an accumulation of olivine (Figure 10). In situ crystallization can explain as well the mineralogical diversity. Unit 1 would be a consequence of the crystallization of the parent magma. Plagioclase would have crystallized as a cumulus mineral whereas clinopyroxene crystallized as a post-cumulus mineral. The residual liquid would thus have been enriched in Fe, Ti and volatiles but not yet in SiO_2 (plagioclase, clinopyroxene and chilled margin have similar SiO_2 contents). A subsequent increase in O_2 fugacity would have forced ilmenite to crystallize [*Pons*, 1982], thus enriching the liquid in SiO_2. This might explain why quartz occurs in proportion as great as 10 vol%. Then, the residual liquid would be enriched in H_2O. This would have forced amphibole to crystallize, which would explain the formation of Unit 6. The alteration of plagioclase observed in Unit 6

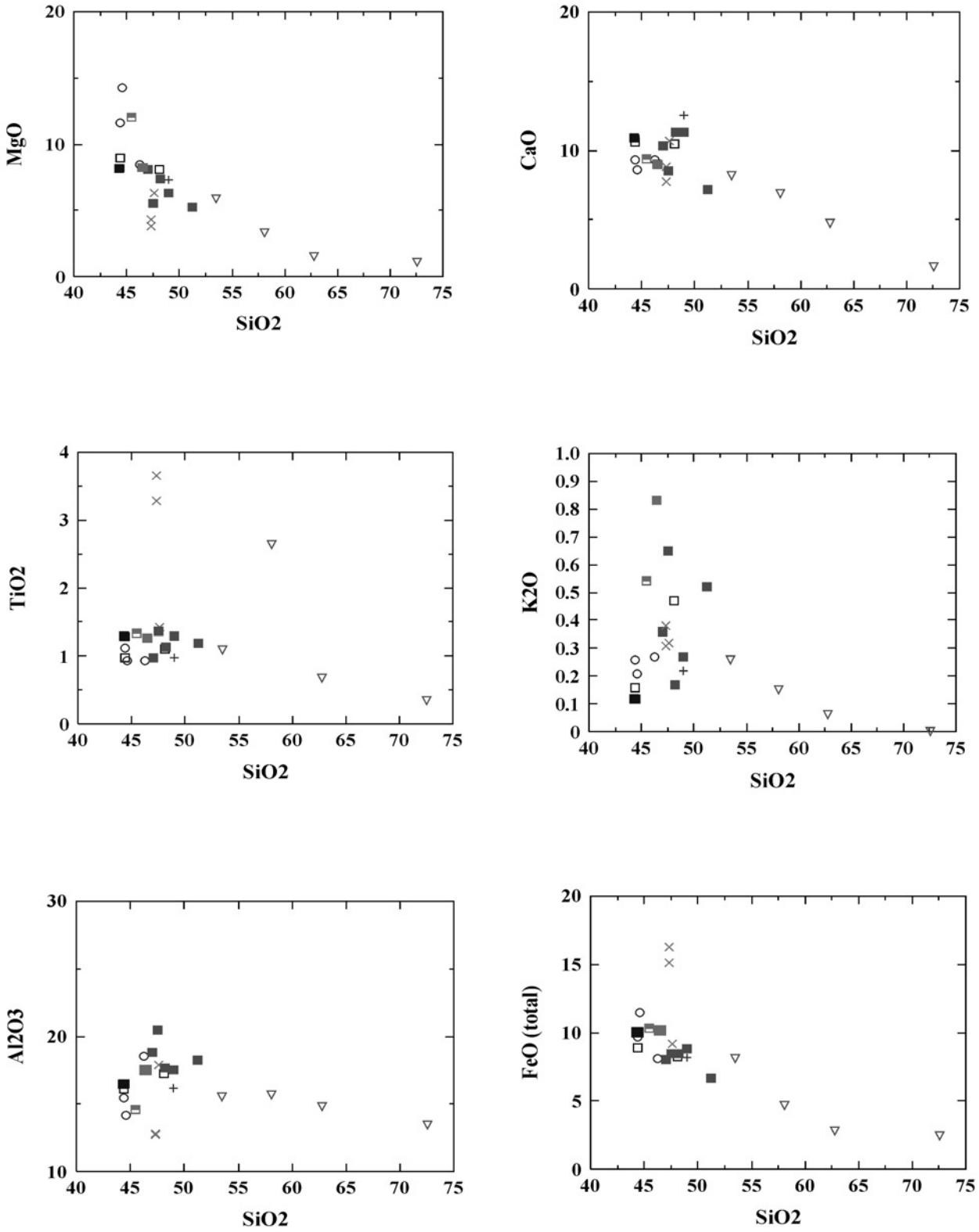

Figure 11. Plot of MgO, CaO, TiO2, K2O, Al2O3, FeOt vs. SiO2 (in wt %) for Marziqallal rocks. See Figures 6 and 7 for symbols.

a)

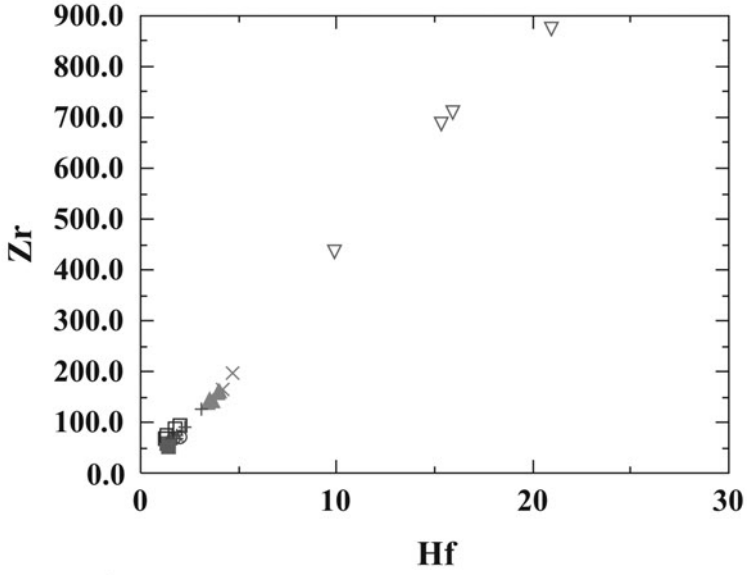
Zr
900.0
800.0
700.0
600.0
500.0
400.0
300.0
200.0
100.0
0.0
0
10
20
30
Hf

b)

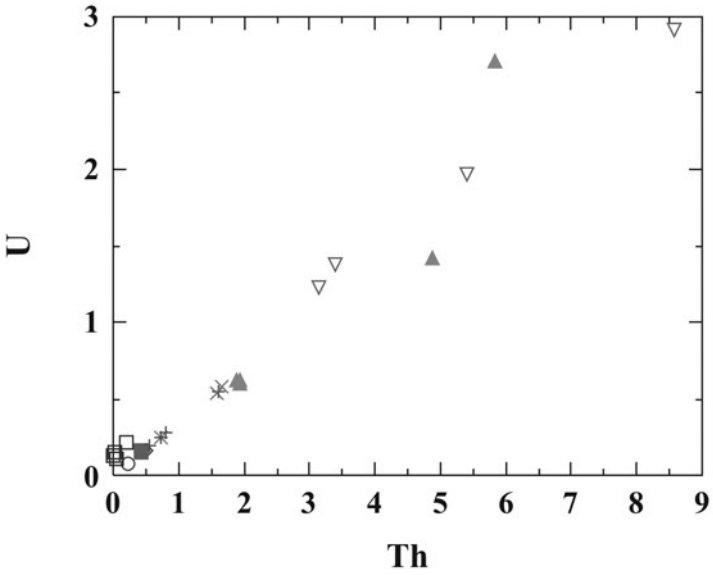
U
3
2
1
0
0
1
2
3
4
5
6
7
8
9
Th

c)

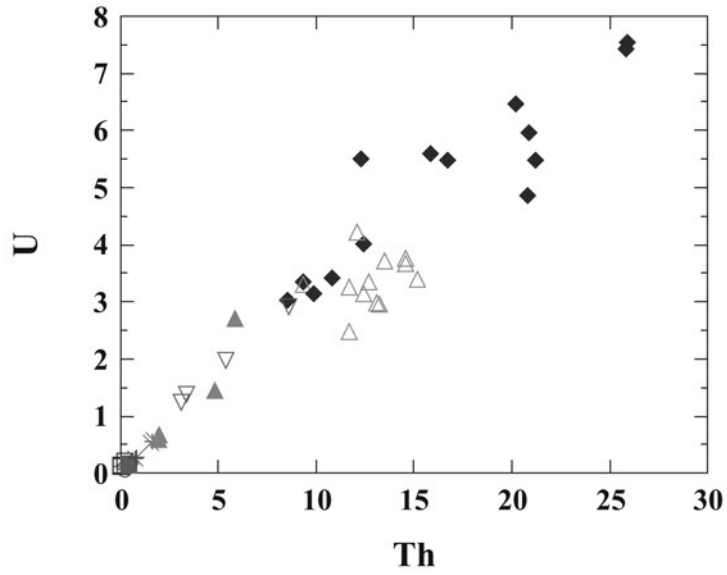
U
8
7
6
5
4
3
2
1
0
0
5
10
15
20
25
30
Th

would have been caused by the presence of late-magmatic fluids. The concentration of olivine in Unit 2 would have been a result of magmatic flow [*Wager and Deer*, 1939; *Irvine*, 1978]. The differentiation of the intrusion did not lead to strong Fe-enrichment, but apparently yielded a granophyric residual liquid.

4.4. Relationship Between Basalts, Cumulates, and Granophyric Veins

[32] As shown above, the rock sequence of the Fourhal area displays the typical patterns of subduction-zone magmas. Clinopyroxene affinities observed in the specific discriminative diagrams of *Leterrier et al.* [1982] are in agreement with the chemical characteristics of the host rock and lie in or very close to the field of orogenic basalts. Although contamination cannot be completely ruled out, a lower degree of partial melting may readily explain that two samples having similar HREE values as the other basalts are more enriched in LREE. The unit 5 and the granophyric rocks, displaying similar Eu negative and Zr, Hf positive anomalies, are typical of more differentiated liquids and suggest an important role of feldspar and accessory zircon during magmatic differentiation of the initial basaltic melt. Figures 12a and 12b show the variation of incompatible element pairs for basalts, granophyric veins and cumulates of the Fourhal area. Both diagrams show Th/U and Zr/Hf correlation coefficients of 0.98 and 1.00, respectively, which is consistent with fractional crystallization [*Joron and Treuil*, 1977, 1989]. Coherence in trace element plots suggests that these continuous trends for the rock suite of the Fourhal do indeed reflect liquid lines of descent, compatible with a cogenetic suite.

4.5. Basaltic Magma Emplacement

[33] Structural and sedimentological evidence shows that the pillow lavas basalts, the gabbroic sills and the granophyric veins emplaced during thrusting. The synchronism in the emplacement of basalts and plutonic sills/veins is corroborated by the co-genetism of the magmas. These magmas may have reached the intrusion level by rising through a network of pre-existing or newly formed faults and shear zones oriented at low angle to the direction of regional shortening so as to open during the propagation of the thrust wedge. The faults formed during the pre-Visean transtension [*Piqué et al.*, 1993] could be good candidates. Then, the magmas intruded laterally along bedding and other discontinuities to form the sills or erupted at the surface as lava flows. The physical possibility of magma intrusion through faults and shear zones has been thoroughly discussed by *Brown and Solar* [1998] who considered that shear zones, even oriented at high angle to the direction of contraction, constitute a favored way of access of magmas to the upper levels. Therefore, the sills and veins can be considered as batches of basaltic magma en route to the surface during contractional deformation, which have locally been impeached to rise further. This may explain their in situ evolution and crystallization.

4.6. Comparison With the Other Early Carboniferous Intrusive Rocks of the Moroccan Mesetas

[34] Pillow lava basalts interbedded with Visean to Early Westphalian syntectonic "flysch" deposits similar to those in the Fourhal area have been observed in the whole Western and Eastern Mesetas. On AFM plots, all the samples from the Eastern and Western Mesetas analyzed by *Kharbouch* [1994] lie in the same calc-alkaline field as the basalts, gabbros and dolerites of the Fourhal basin studied in the present paper (Figure 6). Although only major elements are considered in these diagrams, it can be reasonably inferred that calc-alkaline basaltic magmatism was the rule in the Moroccan Mesetas during the development of the syncontractional foreland basin.

[35] In addition to basaltic pillow lavas and sills/veins, a calc-alkaline suite containing coeval potassic (shoshonitic) and sodic series has been recognized in the Tanncherfi plutonic complex in the Eastern Meseta [*Ajaji et al.*, 1998]. This plutonic complex dated of 344 ± 6Ma, i.e., Middle Visean, from Rb-Sr measurements [*Ajaji et al.*, 1998] also intruded during Visean compression [*Bouabdelli and Piqué*, 1996; *Ben Abbou et al.*, 2001]. On a U vs. Th plot, the points representing the Tanncherfi intrusion are well-correlated (correlation coefficient of 0.98) with those representing the basalts, gabbros, dolerites and granophyric veins analyzed herein (Figure 12c), which suggests a same source to the magmas.

5. Discussion

5.1. Geodynamic Setting of the Foreland Basin

[36] Subduction-related syncontractional foreland basins may develop in a prolithospheric setting or a retrolithospheric setting [*Beaumont et al.*, 1996; *Catuneanu et al.*, 1997]. In the Moroccan Meseta, there is no direct evidence of the direction of dip of the downgoing plate but the presence of syncontractional foreland basin magmatism may provide indirect evidence. According to *Wilson* [1993, p. 9], partial melting of the upper mantle may occur in three ways: (1) addition of volatiles reducing the temperature of partial melting at a given pressure (wet melting); (2) increase in potential temperature of the mantle; and (3) adiabatic upwelling of the asthenosphere to depths lower than 50 km (decompression melting) [*McKenzie and Bickle*, 1988; *Wilson*, 1989, 1993].

[37] In a pro-lithospheric setting, only decompression melting might be envisaged since neither volatile nor heat sources are expected beneath the downgoing plate. Magma-

Figure 12. (opposite) Plots of incompatibles element pairs. (a) Plot of Zr vs. Hf for samples from the Fourhal area; (b) Plot of U vs. Th. for samples from the Fourhal area; and (c) Plot of U vs. Th. for Fourhal magmatism (this paper) and Tanncherfi intrusion [after *Ajaji et al.*, 1998]. △ : sodic series (including quartz monzodiorites, granodiorites); ✦ : potassic series (including monzogabbros, quartz monzonites, monzogranites). Other symbols in Figures 6 and 7.

tism in Abor and Iberian Pyrite Volcanic Belt has been attributed to partial melting underneath the proforeland basin [*Sengupta et al.*, 1996; *Mitjavila et al.*, 1997]. Some authors [e.g., *Giraud and Didier*, 1981; *Boyet et al.*, 2001] interpreted in a similar way the volcanic detritus in the Taveyannaz-Champsaur-Annot sandstones as resulting from in situ volcanism, whereas others [*Von Blanckenburg and Davies*, 1995; *Sinclair*, 1997] believe these to have been issued from volcanoes situated close to, and in both sides of, the suture. In the Abor window, decompression at the origin of melting has been ascribed to exaggerated contraction at the vicinity of a collision zone giving rise to lithospheric over-thickening and attendant erosion and asthenosphere upwelling [*Sengupta et al.*, 1996]. This process, however, requires that only a total thickness of 50 km or less, including mantle lithosphere and thickened continental crust, was left by erosion on top of the asthenosphere. This is quite unlikely on a general ground and is obviously not the case in the Moroccan Meseta where the sedimentological study indicates a sub-marine wedge-top depozone and, therefore, a limited erosion of the thickened crust. In the Iberian Pyrite Volcanic Belt, decompression is interpreted as a result of local lithospheric extension in internal syncontractional strike-slip-induced basins [*Mitjavila et al.*, 1997]. This interpretation is hardly sustainable because the lithospheric thinning required to induce asthenospheric melting is much too great to be a result of strike-slip shearing in a contractional setting. Moreover, in the Meseta foreland basin, no strike-slip system was active in the same time as regional contraction, even though strike-slip induced "pull-apart" basins probably existed before [*Piqué et al.*, 1993; *Bouabdelli and Piqué*, 1996]. It might also be envisaged that lithospheric extension could occur in front of a contractional foreland basin as suggested by *Milani et al.* [1999]. In this case, however, neither the basaltic lavas could be interlayered with the thrust-related deposits nor the sills intruded along these strata as observed in the Moroccan Meseta. Lithospheric delamination [*Bird*, 1979] is also unlikely since this process cannot have produced basaltic magmas in the contracted part of the orogen [see, e.g., *Channell and Mareschal*, 1989, Figures 3, 5, and 7]. The andesitic volcanism at the origin of the detritus contained in the Taveyannaz-Champsaur-Annot sandstones has been ascribed to melting beneath the proforeland basin on the basis of (1) the presence of intrusions or lava flows that would have been seen by ancient authors (2) the preservation of the volcanic shape of single-crystal grains and of the angular shape of the detritus, and (3) marks of aerial cooling of lava projections. In fact, basic intrusions or lava flows have not been found since yet [see, e.g., *Giraud and Didier*, 1981; *Boyet et al.*, 2001]. In particular, *Giraud and Didier* [1981, p. 370, l. 15–17] often referred to when the presence of such intrusions/lava flows is invoked clearly indicate that no lava flows have been ever found. Because considerable field work has been done since that time and the exposures are now improved rather than degraded, the presence of basic intrusions/lava flows in the proforeland basin appears quite unlikely. Moreover, the volcanic detritus being transported within turbiditic flows [*Sinclair*, 1992; 1997] the preservation of the volcanic shape of the grains and the angular shape of the clasts can by no way be taken as evidence of short transport and local origin. The marks of aerial cooling of lava detritus identified by *Giraud and Didier* [1981] are in fact additional evidence that these were produced by volcanoes situated in the emerged orogen behind the inner margin of the basin, very close to the suture as shown by *Sinclair*'s [1992, 1997] sedimentological studies. Accordingly, Taveyannaz-Champsaur-Annot volcanism can be considered as relevant to retrolithospheric setting.

[38] The above discussion thus precludes a prolithospheric setting and states that the calc-alkaline magmatism of the Moroccan Mesetas was generated in a retrolithospheric setting as it is the case in most of the subduction-related orogens.

5.2. Lithospheric Processes at the Origin of the Magmatism

[39] In a retrolithospheric setting, the development of a syncontractional foreland basin (retro-foreland basin) implies lithospheric thickening and moderate to shallow angles of subduction. These conditions preclude decompression melting of the asthenosphere. Therefore, if we except the special case of adakitic magmatism, which is thought to derive from melting of a subducted young (<25 Ma) oceanic crust [*Defant and Drummond*, 1990; *Stern and Kilian*, 1996; *Sigmarsson et al.*, 1998; *Martin*, 1999], basaltic magmas will only be produced by wet melting of the mantle corner and/or local heating induced by asthenospheric upwelling.

[40] Wet partial melting will occur as a result of hydration and metasomatism of the mantle wedge by volatiles released by the dehydration of the subducted oceanic crust [*Gill*, 1980; *Morris et al.*, 1990; *Sigmarsson et al.*, 1990; *Ishikawa and Nakamura*, 1994; *Plank and Langmuir*, 1993; *Schmidt and Poli*, 1998; *Barragan et al.*, 1998] and possibly by partial melting of the subducted oceanic crust when it is sufficiently young (<25 Ma)[*Defant and Drummond*, 1990; *Bourdon et al.*, 2002]. Dehydration of the subducted oceanic crust is considered to be effective at depths of the subducting slab between 80 and 150 km [*Gill*, 1980; *Tatsumi et al.*, 1986; *Poli and Schmidt*, 1995; *Schmidt and Poli*, 1998] even though the slab dehydrates continuously till depth of about 200 km and water may remain within this slab at greater depths [*Schmidt and Poli*, 1998]. The nature of magmatism generated this way varies from tholeiitic to calc-alkaline and then ultra-potassic (shoshonitic) as a function of the distance from the trench. This change in composition is interpreted as a consequence of either the amount of contamination by the continental crust [*Hildreth and Moorbath*, 1988; *Davidson et al.*, 1990; *Tormey et al.*, 1995] or the nature and/or the amount of fluids released by dehydration of the subducting slab [*Miyashiro*, 1974; *Tatsumi et al.*, 1983, 1986; *Barragan et al.*, 1998; *Schmidt and Poli*, 1998]. According to *Barragan et al.* [1998] or *Schmidt and Poli* [1998], the amount of fluids, which controls the composition of magmas, depends

upon the depth at which these fluids are released. This may explain why in the southern Ecuadorian Andes (1°S to 2°S) where the dip of the subducted slab is rather low (as shown in Figure 3 of *Gütscher et al.* [2000], the slab dips 20° to 5° with an average dip of 12°–14° beneath the arc) arc volcanism occurs from the internal part of the chain (Intra-Andean graben) to the foreland basin (Sub-Andean zone) where ultrapotassic magmas have been recognized [*Barragan et al.*, 1998]. In contrast, in Bolivia where the average slab dip is higher (~30°) volcanoes are restricted to the internal part of the range (Coastal Range to Western Cordillera) [*Dorbath et al.*, 1996; *Rochat et al.*, 1999].

[41] Heating is likely to occur as a consequence of various processes including delamination of the whole lithospheric mantle [*Bird*, 1979], convective removal of the thickened thermal boundary layer [*Houseman et al.*, 1981] and slab breakoff [*Davies and Von Blanckenburg*, 1995; *Von Blanckenburg and Davies*, 1995; *Schmid et al.*, 1996; *Boyet et al.*, 2001]. As discussed by *Von Blanckenburg and Davies* [1995], the first two processes would have generated huge amounts of crustal melts and induced uplifts of large aerial extent and could hardly be at the origin of syncontractional magmatism in orogens such as the Alps where magmatism is confined in a linear zone. These processes are still more unlikely in the Moroccan Meseta where uplifts are limited and of pure tectonic origin and the Hercynian metamorphism nowhere exceeds lower amphibolite facies (no metamorphic domes are observed). Moreover, they are inconsistent with the origin of the magmas by partial melting of the mantle lithosphere recognized in the Moroccan Meseta [*Ajaji et al.*, 1998].

[42] Slab breakoff will occur as a consequence of the resistance of a buoyant lithosphere to the pull forces generated by sinking of the foregoing denser lithosphere [*Davies and Von Blanckenburg*, 1995; *Chemenda et al.*, 2000]. Slab breakoff will cause hot asthenosphere to impinge on the mechanical lithosphere of the overriding plate and induce a deep return flow, thus creating a mechanical/thermal perturbation comparable in many respects with mantle plumes [*Davies and Von Blanckenburg*, 1995]. Heating of the lithospheric mantle by uprising asthenosphere will lead to wet melting of its enriched layers. Slab breakoff is expected to occur at various depths depending on the subduction velocity and slab dip but preferentially at the junction between the denser and the buoyant lithospheres [*Von Blanckenburg and Davies*, 1995; *Mason et al.*, 1998, *Chemenda et al.*, 2000].

5.3. What Origin for the Syncontractional Retroforeland Basin of the Moroccan Hercynides?

[43] As shown above all the magmatism recognized yet in the Moroccan Meseta foreland basin, including not only the basaltic lavas, sill gabbros, doleritic or granophyric veins described in the present study or by *Kharbouch* [1994] but also the Tanncherfi plutonic complex studied by *Ajaji et al.* [1998], is calc-alkaline and syncontractional. This retroforeland basin calc-alkaline magmatism is presently observed at a distance of more than 500 km from the suture. In effect, no evidences of the vicinity of a suture are seen in the Paleozoic and Neoproterozoic terrains situated between the Mesetas and the Mesozoic and recent deposits of the Algerian Maghrebides, or in those of the west of the Bechar area [*Hollard et al.*, 1985].

[44] Calc-alkaline magmatism and the large distance between the suture and the loci of intrusion of the magmas thus suggest a comparison with the Ecuadorian Andes. The production of the calc-alkaline series of the Tanncherfi plutonic complex by partial melting of a continental lithospheric mantle previously enriched in LILE and LREE [*Ajaji et al.*, 1998] and the probable similar origin of the basalts, gabbros, dolerites and granophyric veins studied here (Figure 12) is consistent with dehydration of a subducted slab. Differences are, however, observed between the Moroccan Meseta and Andean volcanic arcs: (1) volcanism, although calc-alkaline and widespread in the foreland basin, is far from having been as active in the Moroccan Meseta as in the Andes; (2) volcanism present in the foreland basin of the Ecuadorian Andes is represented by only few aerial volcanoes in a continental environment [e.g., *Barragan et al.*, 1998] whereas, in the Moroccan Meseta, volcanism only appears as sub-marine lava flows; (3) in the Moroccan Meseta, evidence of volcanic products such as cinerite or volcano-clastics have not been decealed in the foreland basin deposits, which argues against the presence of aerial volcanoes nearer to the suture. Moreover, it is likely that the Moroccan Meseta and the Paleozoic and Neoproterozoic terrains to the east and the south-east represent the prolongation of the South European Variscan belt [*Piqué*, 1981; *Piqué and Michard*, 1989; *Piqué et al.*, 1993; *Matte*, 1986; *Ben Abbou et al.*, 2001] and that continental subduction occurred there as in the rest of the Hercynian orogen.

[45] Calc-alkaline magmatism related to continental subduction has been described in the East Carpathians [*Mason et al.*, 1998; *Seghedi et al.*, 2001], the Alps [see, e.g., *Kagami et al.*, 1991; *Von Blanckenburg and Davies*, 1995; *Schmid et al.*, 1996; *Boyet et al.*, 2001] and in the whole Mediterranean Alpine domain [*Carminati et al.*, 1998]. In the East Carpathians, calc-alkaline magmatism has been ascribed by *Mason et al.* [1998] and *Seghedi et al.* [2001] to subduction-induced dehydration of the oceanic crust as in the general oceanic subduction model and a late alkaline magmatism has been attributed to slab breakoff occurring as the end of the subduction process [*Mason et al.*, 1998]. The East Carpathians, however, fundamentally differ from the Moroccan Meseta since the basin in the overriding plate is extensional (back arc basin) and the volcanic arc restricted to the vicinity of the trench because of the high dip of the subducting slab [*Mason et al.*, 1998; *Seghedi et al.*, 2001]. In contrast, it is well known in the Alps that a compressional retro-foreland basin formed as a result of continental subduction. Partial melting is there attributed either to subduction melting [e.g., *Kagami et al.*, 1991] or slab breakoff [*Von Blanckenburg and Davies*, 1995]. According to the latter authors, slab breakoff is preferable because of the syncollisional nature of this magmatism, since the moment when the continental lithosphere entered the subduction zone coincided with the onset of compression, which in

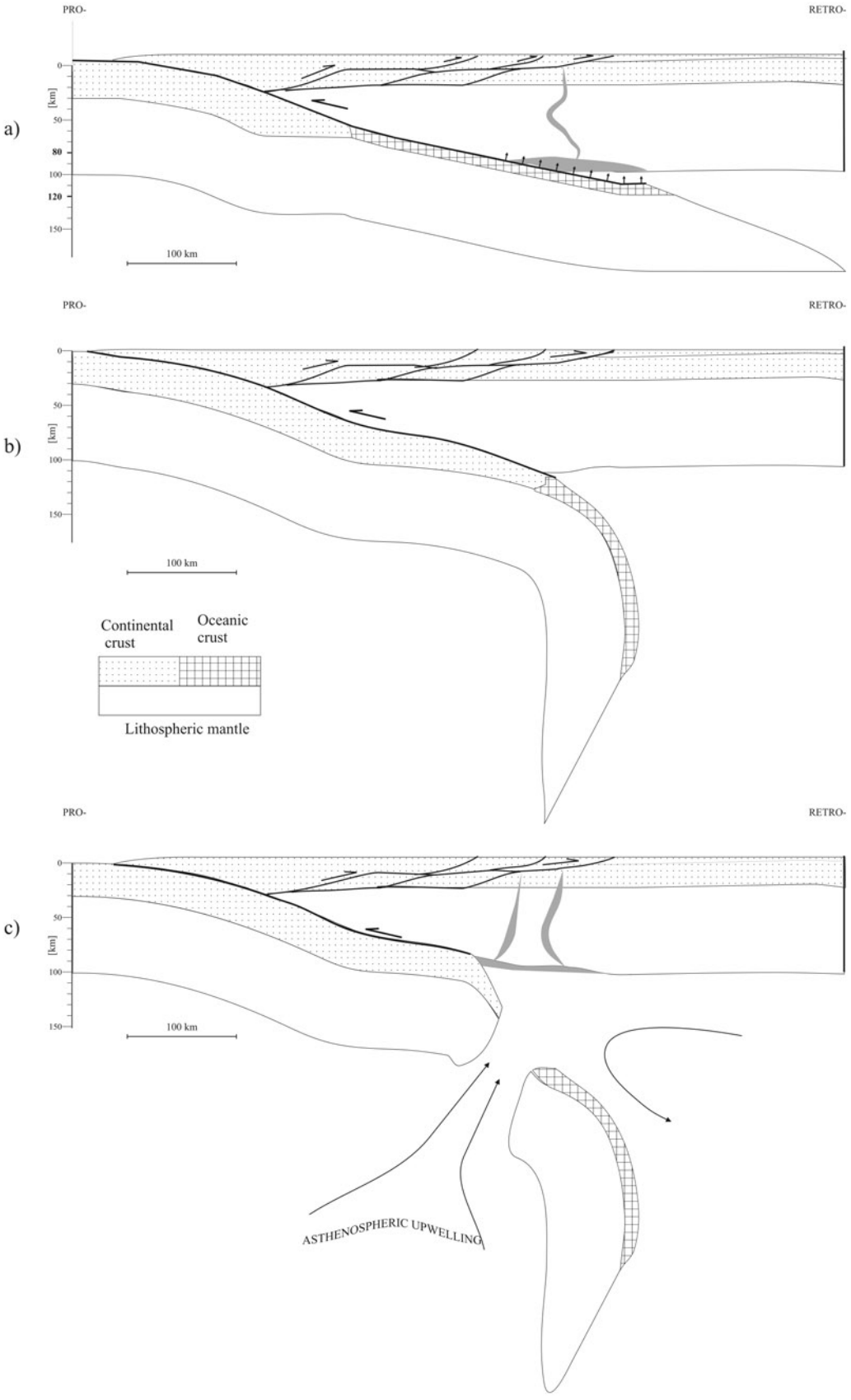
a)
PRO-
RETRO-
[km]
0
50
80
100
120
150
100 km
b)
PRO-
RETRO-
[km]
0
50
100
150
100 km
Continental crust
Oceanic crust
Lithospheric mantle
c)
PRO-
RETRO-
[km]
0
50
100
150
100 km
ASTHENOSPHERIC UPWELLING

the same time should have initiated slab breakoff. The time delay between magmatism and the onset of continental subduction also appears as a similarity between the Moroccan Hercynides and the Alps. In the Alps, this time delay is 10–30 My. In the Western Moroccan Meseta, the products of basaltic magmatism arrived at surface during Early Namurian time (Serpukhovian), i.e., at circa 325–320 Ma, whereas compressional tectonics commenced at least with the Upper Visean, i.e., at circa 340–330 Ma. The inferred time delay is thus of 10–20 My. In the Eastern Meseta, the Tanncherfi complex is slightly older (344 ± 6 Ma) [*Ajaji et al.*, 1998] than the basaltic magmatism in the western Meseta but regional contraction seems to have commenced earlier (Early Visean) in this area even though the ages of ~370 Ma attributed to regional foliation from K-Ar dating of the clay-size fraction [*Huon et al.*, 1987] can be questioned. If the age of 370 Ma is accepted, the time delay between collision and magmatism is of the same order of magnitude (20–30 My) as in the Western Meseta and the Alps.

[46] In spite of these similarities, there are, however, marked differences between the Alpine and the Moroccan Mesetan foreland basins. The subduction-related mafic rocks are found as dikes and pillow lavas in the Moroccan Meseta and not in the Alpine retroforeland basin and the magmatic intrusions crop out at a short distance from the present-day suture in the Alps (at most, 50 km)[see e.g., *Kagami et al.*, 1991; *Von Blanckenburg and Davies*, 1995], whereas the distance to the suture is much greater in the Moroccan Meseta (>500 km).

[47] Starting from the above comparisons, we propose two scenarii for the origin of the foreland basin magmatism in the Moroccan Meseta.

[48] The first scenario involves lithospheric melting induced by subduction-related dehydration of the oceanic crust that pulled down the continental lithosphere (Figure 13a). If we assume that the distance to the suture of the intrusions in the Moroccan Meseta was 500 km and that the depth of origin of the magmas was at most 150 km, and more probably 110–120 km as for the calc-alkaline magmas in the Andes, this yields an average subduction angle of at most 17° and more probably 13°–12°, which is of the same order of magnitude as in the southern Ecuadorian Andes (12°–14°, ~600 km). The shallow subduction angle could explain that the foregoing oceanic lithosphere was brought into ''fertile depths'' beneath the foreland basin and not nearer to the suture. In such a scenario, the time delay of 10–30 Ma. between the arrival of volcanic products at or near the surface and the onset of subduction could be explained by the time spent by the oceanic slab to reach depths of 80–120 km, with a shallow angle of subduction [*Mason et al.*, 1998]. In this case, the subduction rate was at least 2–4 cm y^{-1}.

[49] The second scenario (Figures 13b and 13c) could be that lithospheric melting was a result of slab breakoff as proposed in the Alps by *Von Blanckenburg and Davies* [1995]. The inferred time delay between the intrusion at surface of the magmas and the onset of compression can be interpreted as in the Alps as the time during which slab breakoff and sinking generated asthenospheric flow and heat supply to the base of the mechanical lithosphere [*Von Blanckenburg and Davies*, 1995]. Evidence of slab breakoff-related uplift is provided by the prominence of clastic sedimentation implying the uplift of the orogen and medium to low grade metamorphism as in the western Alps. If slab breakoff was effectively at the origin of magmatism, it must therefore have occurred at some hundred kilometers from the trench as a consequence of either a shallow subduction angle or underplating of the continental lithosphere, or both. On the basis of *Chemenda et al*'s [2000] model experiments (exp. 1), we propose that the foregoing denser oceanic lithosphere first subducted before continental lithosphere entered the subduction zone. Then, its buoyancy forced the continental lithosphere to flatten against the overriding plate. Combined with this upward movement, sinking of the oceanic lithosphere caused it to bend and then to break, thus generating asthenospheric upwelling and partial melting of the lithospheric mantle (Figure 13c). Underplating of the continental lithosphere may also explain why Hercynian regional metamorphism is limited both in extent and grade and no metamorphism is observed even in the exhumed inliers of Neoproterozoic basement. Lithospheric underplating may also explain why the Paleozoic terrains to the east of the foreland basin are poorly deformed and why no large-scale antiformal stacking of deep-seated units formed between the suture and the foreland basin. Eclogitization of the underplating continental crust is likely to have occurred as a result of subduction proceeding with rates such as those (~2–4 cm/y) inferred here [*Bousquet et al.*, 1997]. This may explain why isostasic uplift associated with slab breakoff was limited during the development of the foreland basin as shown by e.g. the submarine wedge-top depozone and the deposition of marine Visean sediments in the Bechar area.

6. Conclusion

[50] The basaltic magmas of the Western Moroccan Meseta formed both pillow lavas flows interbedded with turbiditic and catastrophic sediments deposited in front of a propagating thrust wedge, and doleritic and gabbroic sills that crystallized in situ after having intruded at high temperature along these strata once deposited and lithified. All these magmas are calc-alkaline and co-genetic and emplaced in and during the development of the

Figure 13. (opposite) Possible scenarii for the localization of magmatism in the foreland basin of the Moroccan Mesetas: (a) continental subduction with a shallow subduction angle and dehydration of the foregoing oceanic crust inducing wet melting of the overriding mantle lithosphere. (b and c) Continental subduction and slab breakoff (adapted from *Davies and von Blanckenburg* [1995]). The subducted continental lithosphere flattens against the overriding lithosphere, whereas the foregoing oceanic lithosphere bends and dives more or less vertically. Slab breaks off and the asthenosphere impinges upon overriding lithosphere, which is heated by the deep return flow generated by sinking of the detached slab.

wedge-top depozone of a syncontractional retroforeland basin.

[51] The presence of a syncontractional calc-alkaline foreland basin magmatism can be generalized to the entire Mesetan domain since the other pillow lava basalts interbedded with the same Visean to Early Westphalian syntectonic "flysch" deposits of the Mesetan domain and the acidic to basic rocks of the Visean Tanncherfi plutonic complex [*Ajaji et al.*, 1998] are also calc-alkaline and emplaced during the Hercynian compression, although this compression seems to have commenced earlier in the Eastern Meseta (Early Visean) than in the Western Meseta (Middle to Late Visean). Moreover, the Tanncherfi and the Fourhal magmas appear to be co-genetic, which suggests that the basaltic magmas of the pillow lavas and sills were in the same manner as the Tanncherfi a result of wet melting of a metasomatised mantle lithosphere. This origin of the magmas also favors an upper plate setting of the foreland basin.

[52] Because the Moroccan Hercynides are likely to have been a result of continental subduction and the magmatism is observed at a distance of more than 500 km from the suture, it is suggested that the retroforeland basin magmatism was a result of either dehydration of a shallow dipping ($\sim$15°) foregoing oceanic slab, or underplating of the continental lithosphere ending with slab breakoff beneath the foreland basin.

[53] **Acknowledgments.** This work has benefited from numerous stimulating discussions with Mohamed Bouabdelli, José Darrozes, and Patrice Baby. We thank Michel Valladon and Rémy Freydier for their support in the trace elements measurements. We thank two anonymous referees for their constructive reviews. We also thank Midland Valley Ltd. for technical support.

References

Ajaji, T., D. Weis, A. Giret, and M. Bouabdellah, Coeval potassic and sodic calc-alkaline series in post-collisional Hercynian Tanncherfi intrusive complex, north-eastern Morocco: Geochemical, isotopic and geochronological evidence, *Lithos*, *45*, 371–393, 1998.

Allen, P. A., P. Homewood, and G. D. William, Foreland basins: An introduction, in *Foreland Basin*, edited by P. A. Allen and P. Homewood, *Spec. Publ. Int. Assoc. Sedimentol.*, *8*, 3–12, 1986.

Banks, C. J., and J. Warburton, 'Passive-roof' duplex in the frontal structures of the Kirthar and Sulaiman mountain belts, Pakistan, *J. Struct. Geol.*, *8*(3/4), 229–237, 1986.

Barragan, R., D. Geist, M. Hall, P. Larson, and M. Kurz, Subduction controls on the compositions of lavas from the Ecuadorian Andes, *Earth Planet. Sci. Lett.*, *154*, 153–166, 1998.

Beaumont, C., S. Ellis, J. Hamilton, and P. Fullsack, Mechanical model for subduction—Collision tectonics of alpine-type compressional orogens, *Geology*, *24*, 675–678, 1996.

Ben Abbou, M., Dynamique des bassins d'avant-pays carbonifères: Signatures tectoniques, sédimentaires et magmatique de l'évolution de la chaîne hercynienne du Maroc central septentrional. Implications sur le modèle géodynamique de la chaîne hercynienne, thèse ès sciences, 312 pp., Univ. Cadi Ayyad, Marrakech, Morocco, 2001.

Ben Abbou, M., et al., Contrôle tectonique de la sédimentation dans le système de bassins d'avant-pays de la Meseta marocaine, *C. R. Acad. Sci., Ser. IIA*, *332*, 703–709, 2001.

Ben Said, M., H. Termier, G. Termier, and D. Vachard, Le Carbonifère (Viséen supérieur-Bachkirien) entre Bou Chber et Ich ou Mellal (Maroc Central), *Ann. Soc. Géol. Nord*, *XCVIII*, 189–204, 1979.

Ben Said, M., P. Janvier, H. Termier, and G. Termier, Présence du Westphalien inférieur dans le série de Fourhal (Maroc Central), *C. R. Acad. Sci., Ser. IIA*, *290*, 1329–1332, 1980.

Bird, P., Continental delamination and the Colorado Plateau, *J. Geophys. Res.*, *84*, 7561–7571, 1979.

Bouabdelli, M., and A. Piqué, Du bassin sur décrochement au bassin d'avant-pays: Dynamique du bassin d'Azrou-Khénifra (Maroc hercynien central), *J. Afr. Earth Sci.*, *23*, 213–222, 1996.

Bourdon, E., J. P. Eissen, M. Monzier, C. Robin, H. Martin, J. Cotten, and M. L. Hall, Adakite-like lavas from Antisana volcano (Ecuador): Evidence for slab melt metasomatism beneath the Andean Northern Volcanic Zone, *J. Petrol.*, *43*, 199–217, 2002.

Bousquet, R., B. Goffé, P. Henry, X. Le Pichon, and C. Chopin, Kinematic, thermal and petrological model of the central Alps: Lepontine metamorphism in the upper crust and eclogitisation of the lower crust, *Tectonophysics*, *273*, 105–127, 1997.

Boyet, M., H. Lapierre, M. Tardy, D. Bosch, and R. Maury, Nature des sources des composants andésitiques des Grès du Champsaur et des Grès de Taveyannaz: Implications dans l'évolution des Alpes occidentales au Paléogène, *Bull. Soc. Geol. Fr.*, *172*, 487–501, 2001.

Brown, M., and G. S. Solar, Granite ascent and emplacement during contractional deformation in convergent orogens, *J. Struct. Geol.*, *20*, 1365–1393, 1998.

Carminati, E., M. J. R. Wortel, W. Spakman, and R. Sabadini, The role of slab detachment processes in the opening of the western-central Mediterranean basins: Some geological and geophysical evidence, *Earth Planet. Sci. Lett.*, *160*, 651–665, 1998.

Catuneanu, O., C. Beaumont, and P. Waschbusch, Interplay of static loads and subduction dynamics in foreland basins: Reciprocal stratigraphies and "missing" peripheral bulge, *Geology*, *25*, 1087–1090, 1997.

Channell, J. E. T., and J. C. Mareschal, Delamination and asymmetric lithospheric thickening in the development of the Tyrrhenian Rift, in *Alpine Tectonics*, edited by M. Coward, *Geol. Soc. Spec. Publ.*, *45*, 285–302, 1989.

Chemenda, A. I., J.-P. Burg, and M. Mattauer, Evolutionary model of the Himalaya-Tibet system: Geopoem based on new modelling, geological and geophysical data, *Earth Planet. Sci. Lett.*, *174*, 397–409, 2000.

Davidson, J. P., N. J. McMillan, S. Moorbath, G. Wörner, R. S. Harmon, and L. Lopez-Escobar, The Nevados de Pachayata volcanic region (18°S/69°W, n. Chile), II, Evidence for widespread crustal involvement in Andean magmatism, *Contrib. Mineral. Petrol.*, *105*, 412–432, 1990.

Davies, J. H., and F. von Blanckenburg, Slab breakoff: A model lithosphere detachment and its test in magmatism and deformation of collisional orogens, *Earth Planet. Sci. Lett.*, *129*, 85–102, 1995.

DeCelles, P. G., and K. A. Giles, Foreland basin systems, *Basin Res.*, *8*, 105–123, 1996.

Defant, M. J., and M. S. Drummond, Derivation of some modern arc magmas by melting of young subducted lithosphere, *Nature*, *347*, 662–665, 1990.

Dorbath, C., and A. Paul, A tomography of the Andean crust and mantle at 20°S: First results of the Lithoscope Experiment, *Phys. Earth. Planet. Inter.*, *97*, 133–144, 1996.

Duke, W. L., Geostrophic circulation or shallow marine turbidity currents? The dilemma of paleoflow patterns in storm-influenced prograding shoreline systems, *J. Sediment. Petrol.*, *60*, 870–883, 1990.

Gill, J., *Orogenic Andesites and Plate Tectonics*, 390 pp., Springer-Verlag, New York, 1980.

Giraud, J. D., and J. Didier, Présence de manifestations volcaniques autochtones à la base des grès de Taveyanne du secteru de Flaine-l'Albaron (Haute-Savoie, France), *C. R. Acad. Sci., Ser. IIA*, *292*, 369–372, 1981.

Gütscher, M.-A., W. Spakman, H. Bijwaard, and E. R. Engdahl, Geodynamics of flat subduction: Seismicity and tomographic evidence from the Andean margin, *Tectonics*, *19*, 814–833, 2000.

Hildreth, W. E., and S. Moorbath, Crustal contribution to arc magmatism in the Andes of central Chile, *Contrib. Mineral. Petrol.*, *98*, 455–499, 1988.

Hollard, H., et al., Carte géologique du Maroc, scale 1/1,000,000, *Notes Mém. Serv. Géol. Morocco*, *260*, 1985.

Houseman, G. A., D. P. McKenzie, and P. Molnar, Convective instability of a thickened boundary layer and its relevance for the thermal evolution of continental convergent belts, *J. Geophys. Res.*, *86*, 6115–6132, 1981.

Huon, S., A. Piqué, and N. Clauer, Etude de l'Orogenèse hercynienne au Maroc par la datation K-Ar de l'évolution métamorphique de schistes ardoisiers, *Sci. Geol. Bull.*, *40*(3), 273–284, 1987.

Irvine, T. N., Density current structure and magmatic sedimentation, *Year Book Carnegie Inst. Washington*, *77*, 717–725, 1978.

Irvine, T. N., Terminology for Layered intrusions, *J. Petrol.*, *23*, 127–162, 1982.

Irvine, T. N., and W. R. A. Baragar, A guide to the chemical classification of common volcanic rocks, *Can. J. Earth Sci.*, *8*(5), 523–548, 1971.

Ishikawa, T., and E. Nakamura, Origin of the slab component an arc lavas from across-arc variation of B and Pb isotopes, *Nature*, *370*, 205–208, 1994.

Joron, J. L., and M. Treuil, Utilisation des propriétés des éléments fortement hygromagmaphiles pour l'étude de la composition chimique et de l'hétérogénéité du manteau, *Bull. Soc. Geol. Fr.*, *20*(4), 521–531, 1977.

Joron, J. L., and M. Treuil, Hygromagmaphile element distributions in oceanic basalts as fingerprints of partial melting and mantle heterogeneities: A specific approach and proposal of an identification and modelling method, in *Magmatism in the Ocean Basins*, edited by A. D. Saunders and M. J. Norry, *Geol. Soc. Spec. Publ.*, *42*, 277–299, 1989.

Kagami, H., P. Ulmer, W. Hansmann, V. Dietrich, and R. H. Steiger, Nd-Sr isotopic and geochemical characteristics of the southern Adamello (northern Italy) intrusives: Implications for crustal versus mantle origin, *J. Geophys. Res.*, *96*, 14,331–14,346, 1991.

Kharbouch, F., Les laves devono-dinantiennes de la Meseta marocaine: Étude petro-geochimique et implication geodynamique, Thèse ès sciences, 268 pp., Univ. de Bretagne Occidentale, Brest, France, 1994.

Leterrier, J., R. C. Maury, P. Thonon, D. Girard, and M. Marchal, Clinopyroxene composition as a method of identification of the magmatic affinities of paleovolcanic series, *Earth Planet. Sci. Lett.*, *59*, 139–154, 1982.

Martin, H., Adakitic magmas: Modern analogues of Archaean granitoids, *Lithos*, *46*, 411–429, 1999.

Mason, P. R. D., I. Seghedi, A. Szákacs, and H. Downes, Magmatic constraints on geodynamic models of subduction in the East Carpathians, Romania, *Tectonophysics*, *297*, 157–176, 1998.

Matte, P., Tectonics and plate tectonics model for the Variscan belt of Europe, *Tectonophysics*, *126*, 329–374, 1986.

McKenzie, D. P., and M. J. Bickle, The volume and composition of melt generated by extension of the lithosphere, *J. Petrol.*, *29*, 625–679, 1988.

Miall, A. D., *The Geology of Stratigraphic Sequences*, 421 pp., Springer-Verlag, New York, 1997.

Milani, L., L. Beccaluva, and M. Coltorti, Petrogenesis and evolution of the Euganean Magmatic Complex, Veneto region, north east Italy, *Eur. J. Mineral.*, *11*, 379–401, 1999.

Mitjavila, J., J. Marti, and C. Soriano, Magmatic evolution and tectonic setting of the Iberian Pyrite Belt volcanism, *J. Petrol.*, *38*, 727–755, 1997.

Miyashiro, A., Volcanic rock series in island arcs and active continental margins, *Am. J. Sci.*, *274*, 321–355, 1974.

Morris, J. D., W. P. Leemann, and F. Tera, The subducted component in island arc lavas: constraints from Be isotopes and B-Be systematics, *Nature*, *344*, 31–36, 1990.

Nye, C. J., and M. R. Reid, Geochemistry of primary and least fractionated lavas from Okmok volcano, central Aleutians: Implications for arc magma genesis, *J. Geophys. Res.*, *91*, 10,271–10,287, 1986.

Piqué, A., La chaîne hercynienne d'Europe occidentale et son prolongement dans le Nord-Ouest de l'Afrique, *Sci. Géol. Bull.*, *34*, 123–134, 1981.

Piqué, A., and A. Michard, Moroccan hercynides: A synopsis. The Paleozoic sedimentary and tectonic evolution at the northern margin of West Africa, *Am. J. Sci.*, *289*, 286–330, 1989.

Piqué, A., G. Bossière, J.-P. Bouillin, A. Chalouan, and C. Hoepffner, Southern margin of the Variscan belt: The north-western Gondwana mobile zone (eastern Morocco and northern Algeria), *Geol. Rundsch.*, *82*, 432–439, 1993.

Plank, T., and C. H. Langmuir, Tracing trace elements from sediment input to volcanic output at subduction zones, *Nature*, *362*, 739–743, 1993.

Poli, S., and M. W. Schmidt, H_2O transport and release in subduction zones: Experimental constraints on basaltic and andesitic systems, *J. Geophys. Res.*, *100*, 22,299–22,314, 1995.

Pons, J., Un modèle d'évolution de complexes plutoniques: Gabbros et Granitoïdes de la Sierra Morena Occidentale (Espagne), thèse ès sciences, 429 pp., Univ. Paul Sabatier, Toulouse, France, 1982.

Ricci Lucchi, F., The Oligocene to Recent foreland basins of the northern Apennines, in *Foreland Basin*, edited by P. A. Allen and P. Homewood, *Spec. Publ. Int. Assoc. Sedimentol.*, *8*, 105–141, 1986.

Rochat, P., G. Hérail, P. Baby, and G. Mascle, Crustal balance and control of the erosive and sedimentary processes on the Altiplano formation, *C. R. Acad. Sci., Ser. IIA*, *328*, 189–195, 1999.

Schmid, S. M., O. A. Pfiffner, N. Froitzheim, G. Schönborn, and E. Kissling, Geophysical-geological transect and tectonic evolution of the Swiss-Italian Alps, *Tectonics*, *15*, 1036–1064, 1996.

Schmidt, M. W., and S. Poli, Experimentally based water budgets for dehydrating slabs and consequences for arc magma generation, *Earth Planet. Sci. Lett.*, *163*, 361–379, 1998.

Seghedi, I., H. Downes, Z. Pécskay, M. F. Thirlwall, A. Szakacs, M. Prychodko, and D. Mattey, Magmagenesis in a subduction-related post-collisional volcanic arc segment: The Ukrainian Carpathians, *Lithos*, *57*, 237–262, 2001.

Sengupta, S., S. K. Acharyya, and J. B. De Smeth, Geochemical characteristics of the Abor volcanic rocks, NE Himalaya, India: Nature and early Eocene magmatism, *J. Geol. Soc. London*, *153*, 695–704, 1996.

Sigmarsson, O., M. Condomines, J. D. Morris, and R. S. Harmon, Uranium and 10 Be enrichments by fluids in the Andean arc magmas, *Nature*, *346*, 163–165, 1990.

Sigmarsson, O., H. Martin, and J. Knowles, Melting of a subducted oceanic crust from U-Th disequilibria in austral Andean lavas, *Nature*, *394*, 566–569, 1998.

Sinclair, H. D., Turbidite sedimentation during Alpine thrusting: The Taveyannaz sandstones of eastern Switzerland, *Sedimentology*, *39*, 837–856, 1992.

Sinclair, H. D., Tectono-stratigraphic model for underfilled peripheral foreland basins: An Alpine perspective, *Geol. Soc. Am. Bull.*, *109*, 324–346, 1997.

Sinclair, H. D., Delta-fed turbidite systems of the French alpine foreland basin: A new depositional model for the Annot sandstones, *J. Sediment. Res.*, *70*, 504–519, 2000.

Smith, I. E. M., T. J. Worthington, R. C. Price, and J. A. Gamble, Primitive magmas in arc-type volcanic associations: Examples from the southwest Pacific, *Can. Mineral.*, *35*, 257–273, 1997.

Souquet, P., R. Eschard, and H. Lods, Facies sequences in large-volume debris-and-turbidity flow deposits from the Pyrenees (Cretaceous; France, Spain), *Geomar. Lett.*, *7*, 83–90, 1987.

Stern, C. R., and R. Kilian, Role of the subducted slab, mantle wedge and continental crust in the generation of adakites from the Andean Austral Volcanic Zone, *Contrib. Mineral. Petrol.*, *123*, 263–281, 1996.

Sun, S. S., and W. F. McDonough, Chemical and isotopic systematics of oceanic basalts, implications for mantle composition processes, in *Magmatism in the Ocean Basins*, edited by A. D. Saunders and M. J. Norry, *Geol. Soc. Spec. Publ.*, *42*, 313–345, 1989.

Tatsumi, Y., M. Sakuyama, H. Fukuyama, and I. Kushiro, Generation of arc basalt magmas and thermal structure of the mantle wedge in subduction zones, *J. Geophys. Res.*, *88*, 5815–5825, 1983.

Tatsumi, Y., D. L. Hamilton, and R. W. Nesbitt, Chemical characteristics of fluid phase released from a subducted lithosphere and origin of arc lavas: Evidence from high-pressure experiments and natural rocks, *J. Volcanol. Geotherm. Res.*, *29*, 293–309, 1986.

Termier, H., *Etude Géologique sur le Maroc Central et le Moyen-Atlas Septentrional*, *Notes Mém. 33*, 1566 pp., Serv. Mineral. et Cartes Géol. Maroc, Marrakech, Morroco, 1936.

Tormey, D. R., F. A. Frey, and L. Lopez-Escobar, Geochemistry of the active Azufre-Planchon-Peteroa volcanic complex, Chile (35°15′S): Evidence for multiple sources and processes in a cordilleran arc magmatic system, *J. Petrol.*, *36*, 265–298, 1995.

Von Blanckenburg, F., and J. H. Davies, Slab breakoff: A model for syncollisional magmatism and tectonics in the Alps, *Tectonics*, *14*, 120–131, 1995.

Wager, L. R., and W. A. Deer, Geological investigations in East Greenland, part III, The petrology of the Skaergaard Intrusion, Kangerdlugssuaq, E. Greenland, *Medd. Groenl.*, *105*(4), 1939.

Walker, R. G., and A. G. Plint, Wave and storm dominated shallow marine systems, in *Facies Models: Response to Sea Level Change*, edited by R. G. Walker and N. P. James, pp. 224–225, Geol. Assoc. Can., St John's, Newfoundland, 1992.

Wilson, M., *Igneous Petrogenesis*, 466 pp., Unwin Hyman, Boston, Mass., 1989.

Wilson, M., Magmatism and the geodynamics of basin formation, *Sediment. Geol.*, *86*, 5–29, 1993.

D. Béziat, S. Brusset, F. Christophoul, P. Debat, J. Déramond, M. Roddaz, and J.-C. Soula, Laboratoire de Mécanisme des Transferts en Géologie, UMR 5563, Université Paul Sabatier, 38 rue des 36 ponts, F-31400, Toulouse, France. (dbeziat@cict.fr; brusset@cict.fr; christop@cict.fr; petmdebat@wanadoo.fr; deramond@cict.fr; mroddaz@lmtg.ups-tlse.fr; jcsoula@cict.fr)

M. Ben Abbou, Y. Driouch, and A. Ntarmouchant, Département de Géologie, Faculté des Sciences, Université Ben Abdallah, Fes, Morocco. (benabbou@hotmail.com; ydriouch@hotmail.com; ntarmouchant.@caramail.com)